Monthly Notices
of the
ROYAL ASTRONOMICAL SOCIETY

MNRAS **482,** 4466–4502 (2019)
Advance Access publication 2018 November 5

doi:10.1093/mnras/sty2999

GASP XIII. Star formation in gas outside galaxies

Bianca M. Poggianti,[1]★ Marco Gullieuszik,[1] Stephanie Tonnesen,[2] Alessia Moretti,[1] Benedetta Vulcani,[1] Mario Radovich,[1] Yara Jaffé,[3] Jacopo Fritz,[4] Daniela Bettoni,[1] Andrea Franchetto,[1,5] Giovanni Fasano,[1] Callum Bellhouse[6] and Alessandro Omizzolo[7]

[1]*INAF – Astronomical Observatory of Padova, vicolo dell'Osservatorio 5, I-35122 Padova, Italy*
[2]*Center for Computational Astrophysics, Flatiron Institute, 162 5th Ave, New York, NY 10010, USA*
[3]*Instituto de Física y Astronomía, Universidad de Valparaíso, Avda. Gran Bretaña 1111 Valparaíso, Chile*
[4]*Instituto de Radioastronomia y Astrofisica, UNAM, Campus Morelia, A.P. 3-72, C.P. 58089, Mexico*
[5]*Dipartimento di Fisica e Astronomia, Universita' di Padova, vicolo dell'Osservatorio 5, I-35122 Padova, Italy*
[6]*University of Birmingham School of Physics and Astronomy, Edgbaston, Birmingham, UK*
[7]*Vatican Observatory, Vatican City, Vatican State*

Accepted 2018 October 31. Received 2018 October 31; in original form 2018 July 13

ABSTRACT

Based on MUSE data from the GASP survey, we study the Hα-emitting extraplanar tails of 16 cluster galaxies at $z \sim 0.05$ undergoing ram pressure stripping. We demonstrate that the dominating ionization mechanism of this gas (between 64 per cent and 94 per cent of the Hα emission in the tails depending on the diagnostic diagram used) is photoionization by young massive stars due to ongoing star formation (SF) taking place in the stripped tails. This SF occurs in dynamically quite cold H II clumps with a median Hα velocity dispersion $\sigma = 27\,\mathrm{km\,s^{-1}}$. We study the characteristics of over 500 star-forming clumps in the tails and find median values of Hα luminosity $L_{\mathrm{H}\alpha} = 4 \times 10^{38}\,\mathrm{erg\,s^{-1}}$, dust extinction $A_V = 0.5$ mag, star formation rate SFR$= 0.003\,\mathrm{M_\odot\,yr^{-1}}$, ionized gas density $n_e = 52\,\mathrm{cm^{-3}}$, ionized gas mass $M_{\mathrm{gas}} = 4 \times 10^4\,\mathrm{M_\odot}$, and stellar mass $M_* = 3 \times 10^6\,\mathrm{M_\odot}$. The tail clumps follow scaling relations ($M_{\mathrm{gas}} - M_*$, $L_{\mathrm{H}\alpha} - \sigma$, SFR-$M_{\mathrm{gas}}$) similar to disc clumps, and their stellar masses are comparable to Ultra Compact Dwarfs and Globular Clusters. The diffuse gas component in the tails is ionized by a combination of SF and composite/LINER-like emission likely due to thermal conduction or turbulence. The stellar photoionization component of the diffuse gas can be due either to leakage of ionizing photons from the H II clumps with an average escape fraction of 18 per cent, or lower luminosity H II regions that we cannot individually identify.

Key words: galaxies: evolution – galaxies: clusters: intracluster medium – galaxies: peculiar.

1 INTRODUCTION

Understanding how stars form would be the key to many of the most pressing astrophysical questions across all fields of research, from cosmology to galaxy evolution to planet formation. The star formation (SF) process is responsible for the generation of energy and chemical elements in the Universe, and is the root of galaxy formation. Star formation is therefore at the heart of astrophysics, and yet it is still a poorly understood phenomenon. The complexity of the physical processes involved, over a wide range of physical scales, still makes a comprehensive theory of star formation a challenging goal in spite of progress (Krumholz 2014). Empirically, a relation between a galaxy's gas content and its SFR (SFrate) is well established (Schmidt 1959; Kennicutt 1998b), and multiwavelength observations of SF at different scales depict a phenomenological description of the relation between interstellar medium phases and SF activity (Kennicutt & Evans 2012), but a thorough understanding of what drives the star formation histories of galaxies must still be developed.

One of the important questions to be answered is what controls the clustering properties of SF. Massive stars form almost exclusively in stellar-cluster-forming clumps (Evans 1999). The clustered and hierarchical structure of star-forming regions depends strongly on the physical conditions in which stars form. Turbulence appears to play an important role (e.g. Elmegreen et al. 2014; Gouliermis et al. 2017) and ambient conditions influence the formation of molecular clouds and their properties as a consequence of radiative, thermal, magneto-hydrodynamical, and dynamical processes. These conditions can greatly vary between galaxies, within individual galaxies, and with redshift, leading to clumps of various sizes and masses (Elmegreen et al. 2013). In the past decade, the characteristics of

★ E-mail: bianca.poggianti@oapd.inaf.it

star-forming clumps at high- and low-z have received a surge of interest, due to the realization that the progenitors of local disc galaxies are high-redshift galaxies in which giant, massive star-forming clumps (10^7–10^9 $M_\odot$) are observed (Elmegreen et al. 2007; Cava et al. 2018).

Probing SF in different regimes, ambient conditions, and epochs is fundamental to obtain an observational picture that can inform our theoretical understanding. For example, the SF conditions in the outskirts of galaxy discs can be substantially different from those in the discs themselves, providing clues about non-linear SF laws and the distribution of stellar masses in the low-SF regime (Elmegreen 2017) and starburst galaxies can help us understand how SF proceeds in the high gas density regime (Kennicutt & Evans 2012).

At the present epoch, most new stars are formed in galaxy discs, but SF is known to take place also in more exotic environments, such as the tidal tails of merging systems (Elmegreen, Kaufman & Thomasson 1993; Bournaud et al. 2004; Schweizer 2006; Boquien et al. 2009; Mullan et al. 2011; Duc 2012; Mulia, Chandar & Whitmore 2015; Vulcani et al. 2017).

In this paper, we investigate the extra-galactic SF occurring in the tails of gas that is being stripped from galaxies, and study the properties of the clumps that form within this gas. Gas can be removed from galaxies by various physical mechanisms, and in clusters the most efficient one is ram pressure stripping, due to the pressure exerted by the hot (10^8 K) intracluster medium (ICM) on the galaxy interstellar medium (ISM) (Gunn & Gott 1972). The ram-pressure-stripped gas can produce tails up to more than 100 kpc long in which new stars can be formed. A summary of both observational and theoretical evidence for this in the literature is deferred until Section 8 to facilitate comparison with the results of this paper.

GASP (GAs Stripping Phenomena in galaxies with MUSE, Poggianti et al. 2017b) is an ESO Large Program aimed at studying processes that remove gas from galaxies. Target galaxies were chosen to have unilateral debris or tails in B-band images, suggestive of gas-only removal, excluding clear mergers and tidal interactions (see Poggianti et al. (2017b). All targets are at redshift $0.04 < z < 0.07$. They are located in different environments (galaxy clusters, groups, filaments, and isolated) and span a wide range of galaxy stellar masses, from 10^9 to $10^{11.5}$ $M_\odot$.

MUSE Integral Field spectroscopy of these galaxies allows us a detailed investigation of the ionized gas phase and the stellar component both in the discs and in the extraplanar tails. This program provides a direct observational window on galaxies in various stages of ram pressure stripping in clusters (Jaffé et al. 2018), from pre-stripping (undisturbed galaxies of a control sample), to initial stripping, peak stripping (Bellhouse et al. 2017; Gullieuszik et al. 2017; Poggianti et al. 2017b; Moretti et al. 2018a), and post-stripping (Fritz et al. 2017), passive and devoid of gas, as well as on a number of physical processes in groups and filaments ranging from stripping to gas accretion, mergers, and cosmic web (Vulcani et al. 2017, 2018a,b, Vulcani et al. MNRAS submitted).

In this paper, we focus on galaxies in clusters, and use the MUSE data to investigate the origin of the ionization of the stripped gas and the SF that takes place within it. After presenting our sample and observations (Section 2) and describing the methods of analysis employed (Section 3), we present our results on ionization mechanisms (Section 4.1) and discuss the location of ongoing SF in Section 4.2. The physical properties of the star-forming clumps (velocity dispersion, Hα luminosity, dust extinction, SFR, gas density, and SFR density, gas mass, and stellar mass) and a few scaling relations linking various properties of the clumps are presented in Section 5. The diffuse component of Hα emission is separately discussed in Section 6, and a summary of global SFR in the discs and tails is given in Section 7. The discussion (Section 8) includes a summary of previous observational results and theoretical expectations, and a summary of our results is given in Section 9.

This paper adopts a Chabrier (2003) IMF and standard concordance cosmology parameters $H_0 = 70\,\mathrm{km\,s^{-1}\,Mpc^{-1}}$, $\Omega_M = 0.3$ and $\Omega_\Lambda = 0.7$.

2 SAMPLE AND OBSERVATIONS

All the observations used in this paper have been obtained from the GASP survey. The GASP sample comprises 64 cluster galaxies that are stripping candidates, plus another 30 candidates in groups, filaments, and isolated and 20 undisturbed galaxies that represent a control sample.

For this work, we have selected galaxies satisfying the following criteria: a) only cluster members; b) with clear tails of extraplanar Hα emitting gas and c) without any nearby companion that could affect the gas morphologies by tidal interactions. In this way, we are excluding galaxies with Hα truncated discs that have gas left only in the central regions of the disc, which are in an advanced phase of stripping (Post-stripping galaxies in Jaffé et al. 2018). An example of such a truncated disc is JO36, studied in detail in Fritz et al. (2017). We are also excluding face-on galaxies with unwinding spiral arms in which, though the gas kinematics clearly indicates stripping, due to the viewing angle no clear gas tails are visible. These are the subject of a dedicated work (Bellhouse et al. MNRAS submitted).

In the following, we will focus on the 16 galaxies with long Hα tails (at least 20 kpc from the disc) complying to the selection criteria described above and observed by GASP at the time of selection, stressing that no additional selection criterion (based, for example, on the gas ionization properties) was employed. Table 1 lists their name, host cluster, redshift and cluster redshift, cluster velocity dispersion, coordinates, and stellar masses.

Observations were carried out in service mode with the MUSE spectrograph mounted at the VLT in wide-field mode with natural seeing. MUSE (Bacon et al. 2010) is an integral-field spectrograph composed of 24 IFU modules with a $4k \times 4k$ CCD each. It has $0.2'' \times 0.2''$ pixels and covers a $1' \times 1'$ field-of-view. It covers the spectral range between 4800 and 9300 Å sampled at 1.25 Å pixel^{-1} with a spectral resolution FWHM = 2.6 Å.

Most of our target galaxies were observed with one MUSE pointing, and some with two pointings in order to cover the length of the tail. On each pointing, 4×675 s exposures were taken in clear, dark-time, $<1''$ seeing conditions. The data were reduced with the most recent available version of the MUSE pipeline (Bacon et al. 2010; http://www.eso.org/sci/software/pipelines/muse), as described in Poggianti et al. (2017b).

3 METHODS

The methods employed to analyse the MUSE data are described in detail in Poggianti et al. (2017b) and are summarized below.

To derive emission line fluxes, velocities, and velocity dispersions with associated errors we make use of KUBEVIZ (Fossati et al. 2016), an IDL public software that fits Gaussian line profiles using the MPFit package (Markwardt 2009). The MUSE spectral range covers the Hβ, [O III]5007, [O I]6300, H alpha, [N II]6583, [S II]6717, 6731 lines that are of interest for this paper. In our analysis, before performing the fits, we average filter the data cube

Table 1. Sample galaxies. Columns are: (1) GASP ID number from Poggianti et al. (2016); (2) host cluster; (3) galaxy redshift; (4) cluster redshift; (5) cluster velocity dispersion; (6) and (7) RA and DEC; (8) galaxy stellar mass; (9) number of clumps in tail (total number of clumps); (10) references.

ID_{P16}	cluster	z_{gal}	z_{clu}	σ_{clu} (km/s)	RA(J2000)	DEC(J2000)	$M_*(M_\odot)$	$N_{tail\ clumps}$ ($N_{all\ clumps}$)	refs
JO113	A3158	0.0553	0.0594	948	03:41:49.225	−53:24:12.16	$4.7^{5.5}_{3.2} \times 10^9$	4(20)	–
JO135	A3530	0.0542	0.0548	674	12:57:04.322	−30:22:30.19	$1.1^{1.2}_{0.8} \times 10^{11}$	15(77)	(5)
JO141	A3532	0.0588	0.0555	662	12:58:38.371	−30:47:32.31	$4.4^{5.2}_{2.4} \times 10^{10}$	13(55)	–
JO147	A3558	0.0498	0.0486	910	13:26:49.731	−31:23:44.79	$1.3^{1.4}_{0.7} \times 10^{11}$	29(72)	(6)
JO160	A3558	0.0483	0.0486	910	13:29:28.584	−31:39:25.46	$1.1^{1.7}_{0.9} \times 10^{10}$	6(39)	–
JO171	A3667	0.0520	0.0558	1031	20:10:14.753	−56:38:29.49	$3.6^{4.3}_{2.8} \times 10^{10}$	27(93)	(2)
JO175	A3716	0.0468	0.0457	753	20:51:17.593	−52:49:22.34	$3.4^{3.6}_{2.7} \times 10^{10}$	34(80)	(5)
JO194	A4059	0.0410	0.0490	744	23:57:00.740	−34:40:49.94	$1.3^{1.8}_{1.2} \times 10^{11}$	84(223)	(5)
JO201	A85	0.0446	0.0559	859	00:41:30.295	−09:15:45.98	$4.4^{7.8}_{4.1} \times 10^{10}$	57(148)	(4,5,7,8)
JO204	A957	0.0424	0.0451	631	10:13:46.842	−00:54:51.27	$5.5^{6.1}_{3.2} \times 10^{10}$	41(121)	(3,5,8)
JO206	IIZW108	0.0513	0.0486	575	21:13:47.410	+ 02:28:35.50	$7.8^{10.4}_{5.3} \times 10^{10}$	68(139)	(1,5,8)
JO49	A168	0.0450	0.0453	498	01:14:43.924	+ 00:17:10.07	$5.9^{6.3}_{3.5} \times 10^{10}$	6(75)	–
JO60	A1991	0.0623	0.0584	570	14:53:51.567	+ 18:39:04.79	$2.1^{2.9}_{1.5} \times 10^{10}$	17(78)	–
JO95	A2657	0.0433	0.0400	829	23:44:26.659	+ 09:06:54.54	$2.6^{3.3}_{1.4} \times 10^9$	5(46)	–
JW100	A2626	0.0602	0.0548	650	23:36:25.054	+ 21:09:02.64	$2.9^{3.1}_{1.2} \times 10^{11}$	66(131)	(5,8)
JW39	A1668	0.0650	0.0634	654	13:04:07.719	+ 19:12:38.41	$1.6^{1.8}_{1.0} \times 10^{11}$	49(159)	–

Note. Refs: (1) Poggianti et al. (2017b); (2) Moretti et al. (2018a); (3) Gullieuszik et al. (2017); (4) Bellhouse et al. (2017); (5) Poggianti et al. (2017a); (6) Merluzzi et al. (2013); (7) George et al. (2018); (8) Moretti et al. (2018b). Cluster redshifts are taken from Biviano et al. (2017), Moretti et al. (2017), and Cava et al. (2009).

in the spatial direction with a 5 × 5 kernel, corresponding to our worst seeing conditions of 1″ = 0.7–1.3 kpc at the redshifts of our galaxies. The velocity dispersions are corrected for the instrumental line width at each wavelength (see Fumagalli et al. 2014), which at the observed Hα wavelengths of these galaxies is about 46 km s^{-1}.

Before running KUBEVIZ, we correct the MUSE data cube for Galactic extinction and subtract the stellar-only component of each spectrum derived with our spectrophotometric code SINOPSIS (Fritz et al. 2017). SINOPSIS uses the latest SSP models from S. Charlot & G. Bruzual (2018, in preparation) based on stellar evolutionary tracks from Bressan et al. (2012) and stellar atmosphere spectra from a compilation of different authors. SINOPSIS also includes the nebular emission lines for the young SSPs computed with the Cloudy code (Ferland et al. 2013). In addition to the best fit stellar-only model cube that is subtracted from the observed cube, SINOPSIS provides for each MUSE spaxel stellar masses, luminosity-weighted and mass-weighted ages and SF histories in four broad age bins.

All the SFRs in this paper are computed from the H alpha luminosity-corrected both for stellar absorption and for dust extinction, adopting the Kennicutt (1998a)'s relation: SFR($M_\odot$ yr^{-1}) = $4.6 \times 10^{-42} L_{H\alpha}$(erg s^{-1}). The extinction is estimated from the Balmer decrement assuming a value Hα/Hβ = 2.86 and the Cardelli, Clayton & Mathis (1989) extinction law.

The ionized gas density n is derived from the ratio R = [S II]6716/[S II]6731 adopting a gas temperature T = 10 000 K and the calibration of Proxauf, Öttl & Kimeswenger (2014) which is valid for the interval R = 0.4–1.435.

The mass of the ionized gas is estimated as $M_{Mgas} = N_{protons} \times m_H = \frac{L_{H\alpha} \times m_p}{n \alpha_{H\alpha} h\nu_{H\alpha}}$ (Poggianti et al. 2017b), where $L_{H\alpha}$ is the luminosity of the Hα line corrected for stellar absorption and dust extinction, $m_H = 1.6737 \times 10^{-24}$g is the mass of the hydrogen atom, $\alpha_{H\alpha}$ is the effective Hα recombination coefficient (1.17×10^{-13}cm^3 s^{-1}), $h\nu_{H\alpha}$ is the energy of the Hα photon (0.3028×10^{-11}erg) and n is the gas density.

3.1 Definition of tails and Hα clumps

The white-light MUSE images and Hα-flux maps of our sample galaxies are shown in Fig. 1. The black contour is the line we defined to have an estimate of the 'galaxy boundary', as described in Gullieuszik et al. (in prep.). It is computed from the map of the stellar continuum in the Hα region. As a starting point, we used the isophote with a surface brightness 1σ above the average sky background level. This isophote does not have an elliptical symmetry because of the (stellar and gaseous) emission from the stripped gas tails. For this reason, we fit an ellipse to the undisturbed side of the isophote and we replaced the isophote on the disturbed side with the ellipse. In the following. we will refer to the galaxy emission outside of the resulting contour as 'tail'.

All our galaxies present bright Hα knots with logarithmic Hα surface brightness typically between −16.5 and −15 erg s^{-1} cm^{-2} arcsec^{-2}. As discussed throughout this paper, these are star-forming clumps embedded in regions of more diffuse emission. We identify these clumps as described in detail in Poggianti et al. (2017b) using a shell script including IRAF and FORTRAN routines, searching the local minima of the laplace + median filtered Hα MUSE image. The size of these clumps (i.e. their radius, having assumed circular symmetry) is estimated considering outgoing shells until the average counts reach a threshold value that defines the underlying diffuse emission. This radius is therefore an isophotal radius of the kind derived with an isophote method used also in other works (Wisnioski et al. 2012). Isophotal radii are larger than so-called 'core-radii', which are derived as 1σ widths of Gaussian profile fits (see Fig. 1 in Wisnioski et al. 2012). For this work, the Hα flux within each clump is measured including the underlying diffuse emission in which the clump is embedded

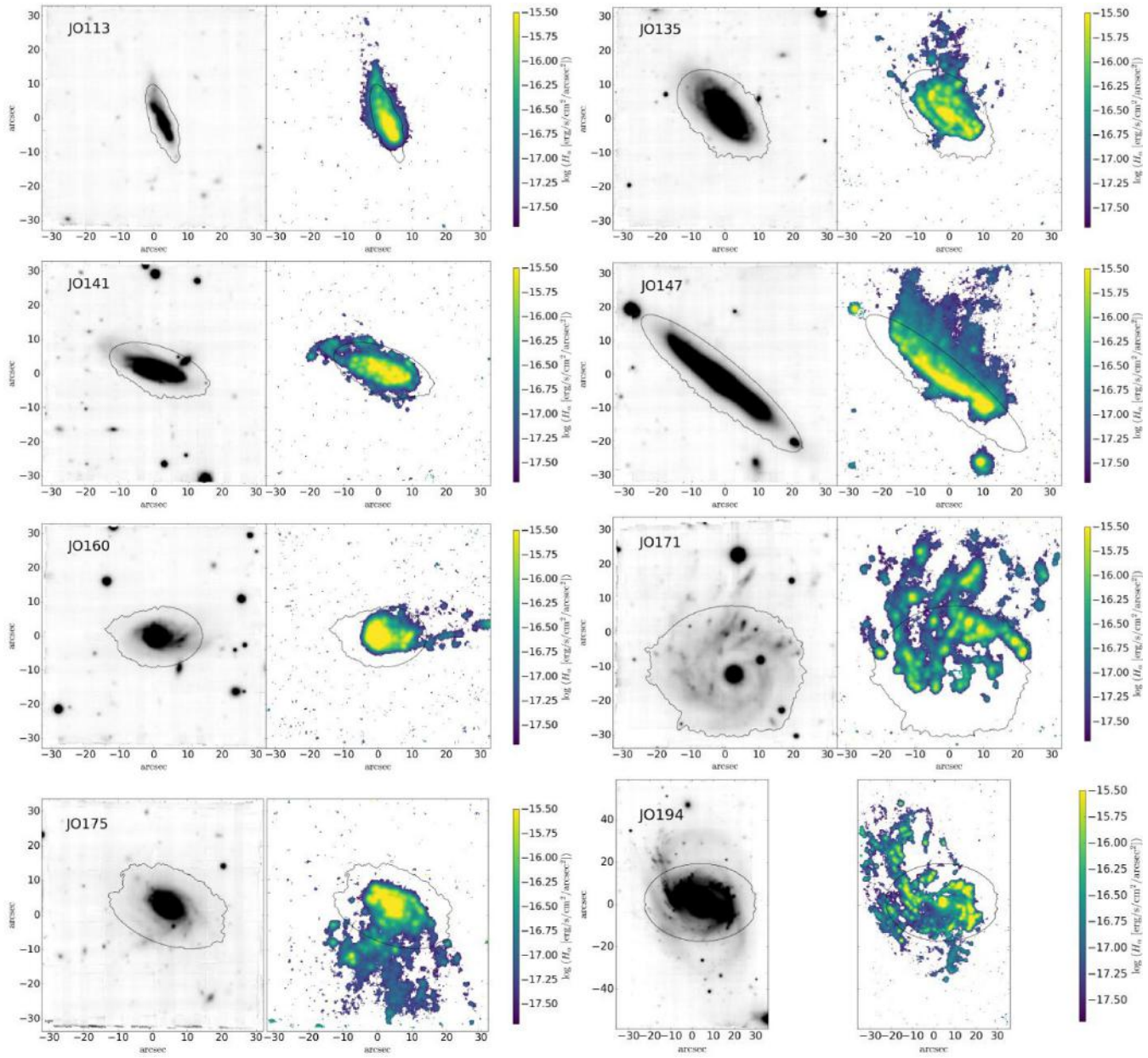

Figure 1. MUSE white image (left) and Hα flux map (right) for each galaxy. Black contours are the stellar contours described in Section 3.1.

and equally sharing the counts of spaxels belonging to overlapping clumps.

4 RESULTS

4.1 Ionization mechanisms

To investigate the gas ionization mechanism, we employ three standard diagnostic diagrams (hereafter DD): [O III]5007/Hβ versus [N II]6583/Hα (N II DD), [O III]5007/Hβ versus [S II]6717,6731/Hα (S II DD) and [O III]5007/Hβ versus [O I]6300/Hα (OI DD).[1] To separate in these diagrams, the regions powered by Star-formation, Composite (SF + LINER/AGN), AGN, and LINER emission, we adopt the division lines by (K03 Kauffmann et al. 2003), (K01 Kewley et al. 2001) (K06 Kewley et al. 2006) and (SB10 Sharp & Bland-Hawthorn 2010).

Fig. 2 presents all three DDs of individual spaxels of each galaxy as well as the galaxy map colour-coded by ionization mechanism. Note that only spaxels in the tails (those outside of the stellar contours) are plotted in the DD, while the map displays both tails and discs.

Only spaxels with an $S/N>3$ in all the four lines used in each diagram are considered in Fig. 2. As a consequence, we can assess the ionization source only for a fraction of the spaxels: the median fraction of Hα luminosity in the tails for which the mea-

[1]For JW100, we have excluded from our analysis the [N II] line which is affected by a sky line.

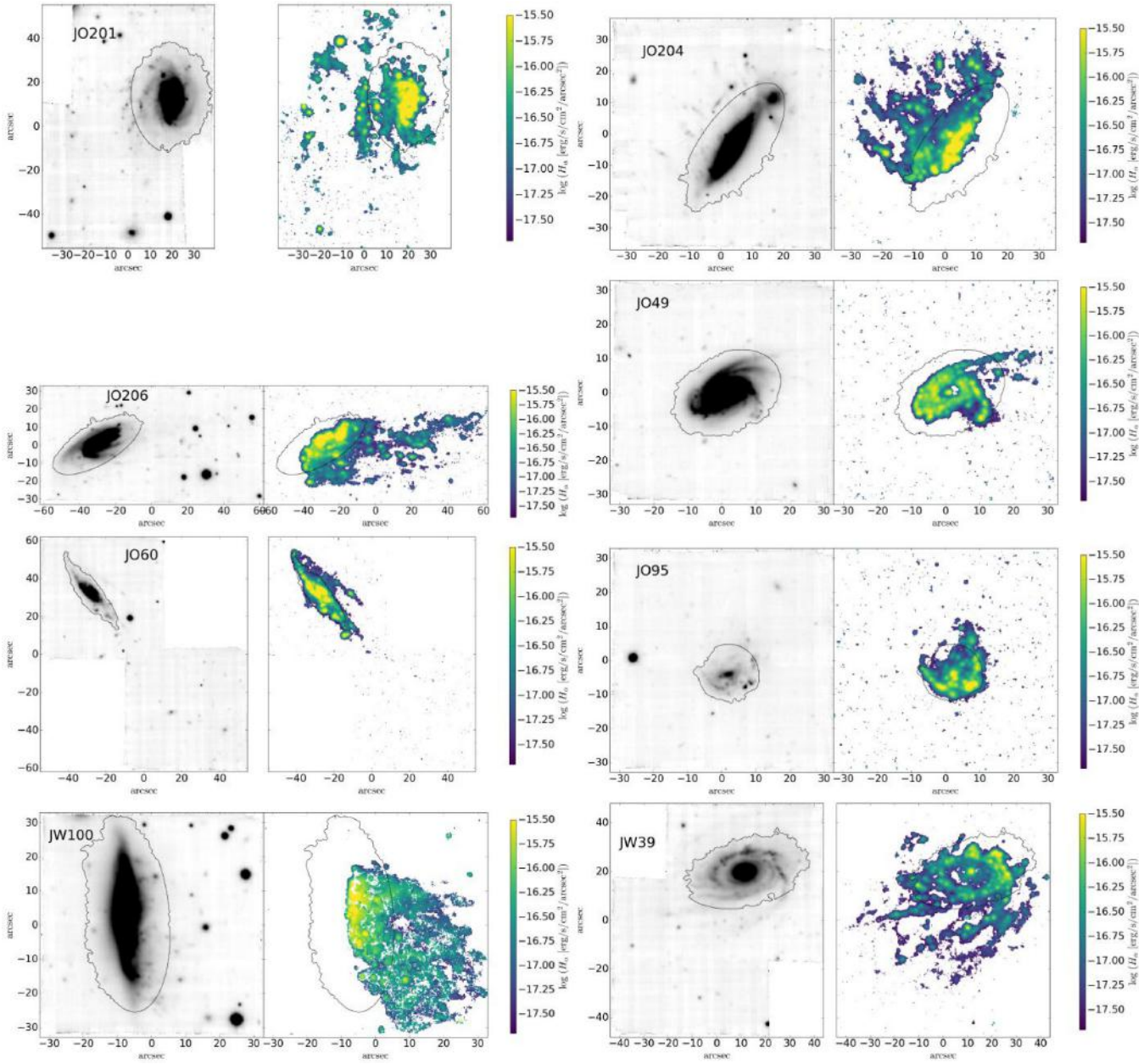

Figure 1. *– Continued*

surement is possible in our sample is 58.0 per cent with a dispersion of 18.7 per cent for the N II DD, 63.6 per cent±14.2 for S II DD, and 57.2 per cent±15.5 for OI DD. Thus, the reader should keep in mind that for about 40 per cent of the Hα luminosity in the tails, the ionization mechanism cannot be determined from DDs because one or more lines are too faint.

We note that for a few of our galaxies there are regions where a single-component Gaussian does not provide a good fit to the observed spectrum, due to the presence of gas at different velocities along the line of sight, or emission around an AGN. The two galaxies for which this effect is more important in the tails are JW100 and JO201, for which detailed diagnostic diagrams based on two Gaussian component fits were presented in Poggianti et al. (2017a) and Bellhouse et al. (submitted), respectively. Since we have verified that in the tails (that are the subject of the current paper) the single-component fit yields DD results very similar to the double component, hereafter we only show the single-component results.

From the spaxel-by-spaxel analysis of Fig. 2, a number of conclusions can be drawn.

For the majority of galaxies, the N II DD and and S II DD generally show an excellent agreement, and they indicate SF as the predominant ionization mechanism in the tails (in JO113, JO141, JO160, JO171, JO175, JO201, JO204, JO206, JO49, JO60, JO95, JW100, JW39 plus JO147, and JO194 from S II DD) or an SF + Composite origin (N II DD for JO194, and especially for JO147).

In contrast, a non-negligible fraction of spaxels in the tails of all galaxies has an [O I]/Hα ratio that is too high for being powered

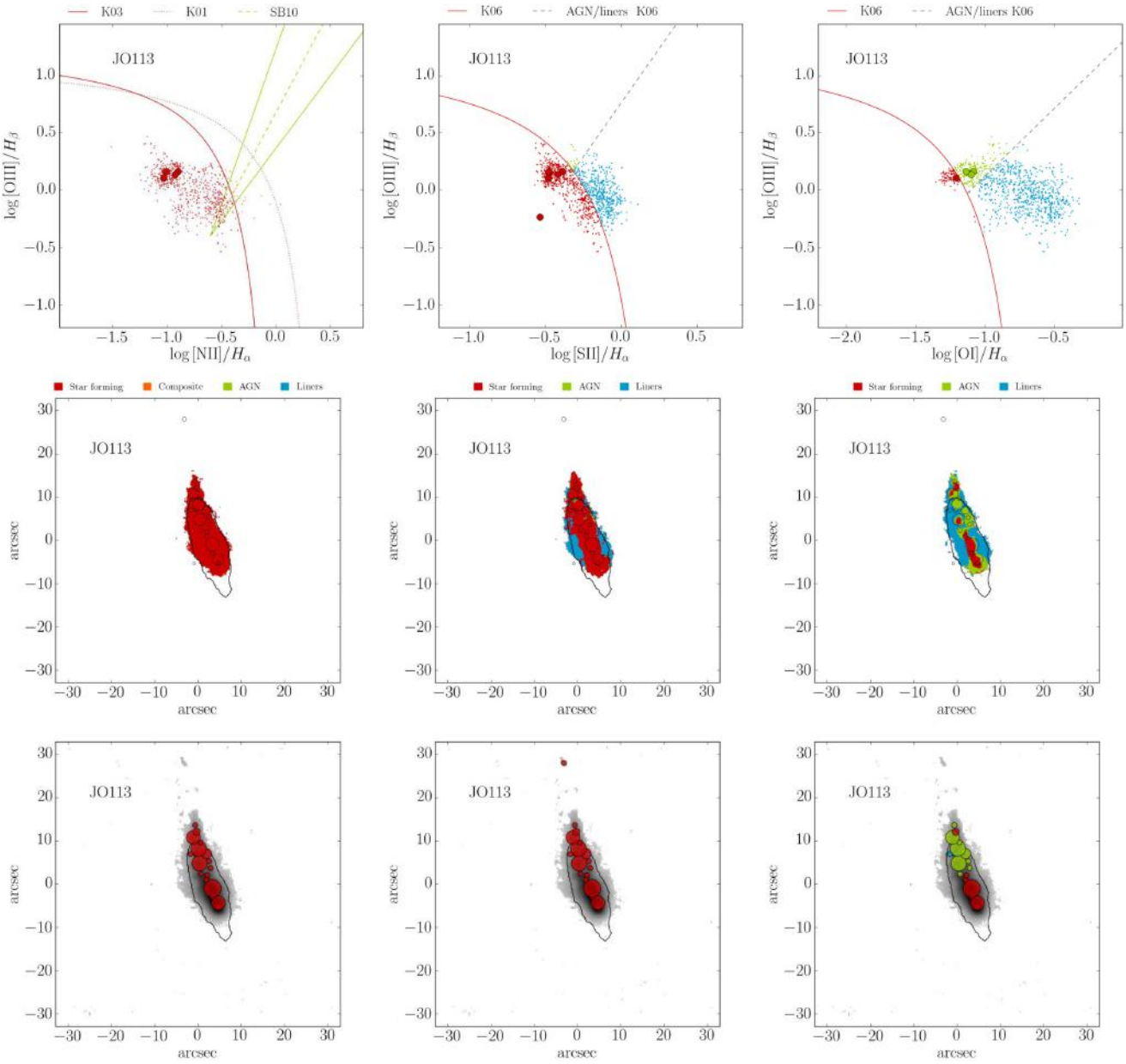

Figure 2. Diagnostic diagram results: N II DD (left), S II DD (centre) and OI DD (right). For each galaxy: Top panels: DDs for individual spaxels (small points) and clumps (large circles); Middle panels: spaxel map colour-coded for ionization mechanism (see legend on top of middle panels) with clump contours and stellar contours overplotted; Bottom panels: colour-coded map of the clumps with stellar contour overplotted. The diagrams include only spaxels and clumps in the tails, i.e. that are outside of the line contour showing the stellar disc (see text for details). Only spaxels with an $S/N>3$ in all the four lines used are plotted. See footnote 1) for JW100.

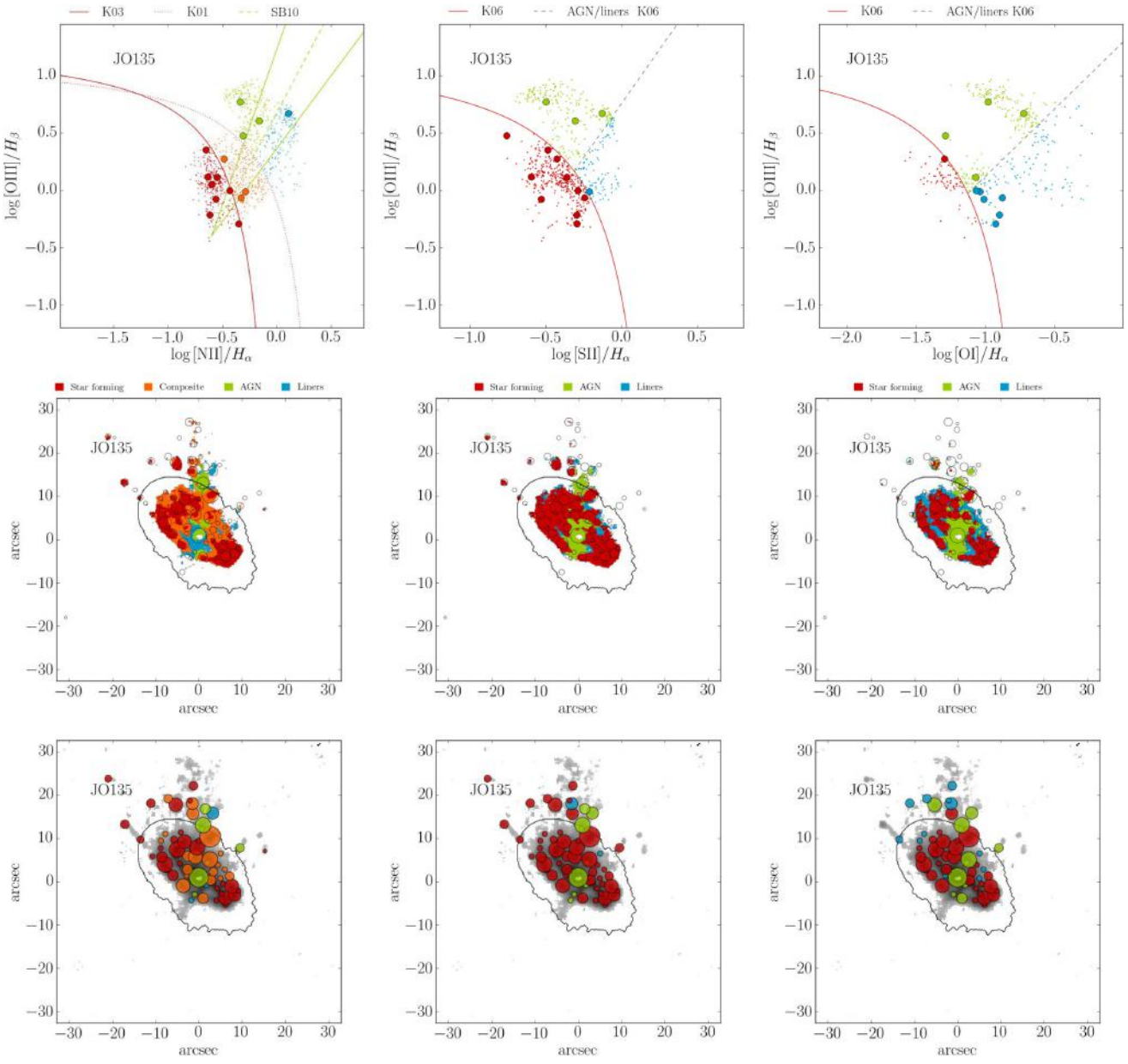

Figure 2. *– Continued*

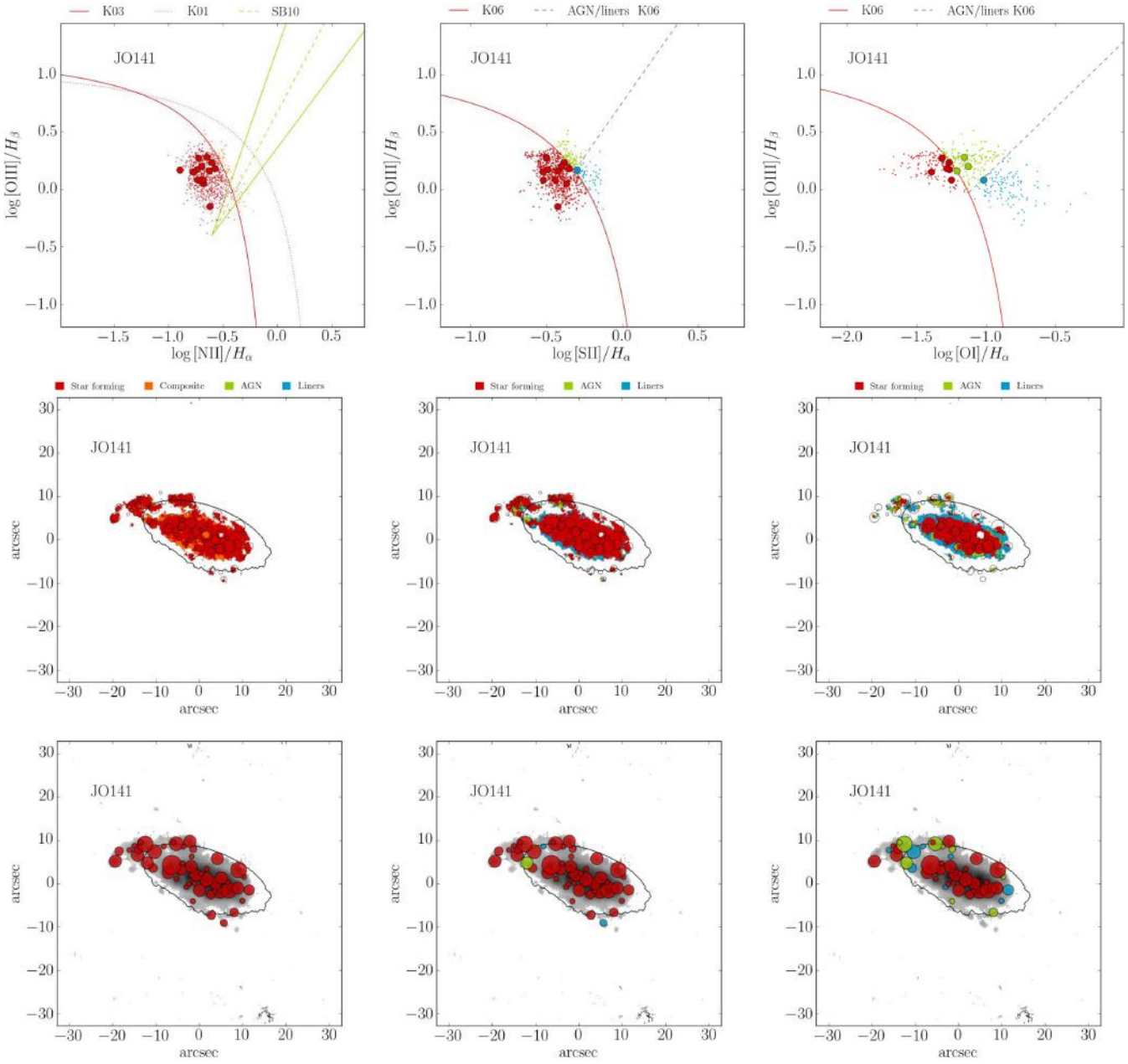

Figure 2. – *Continued*

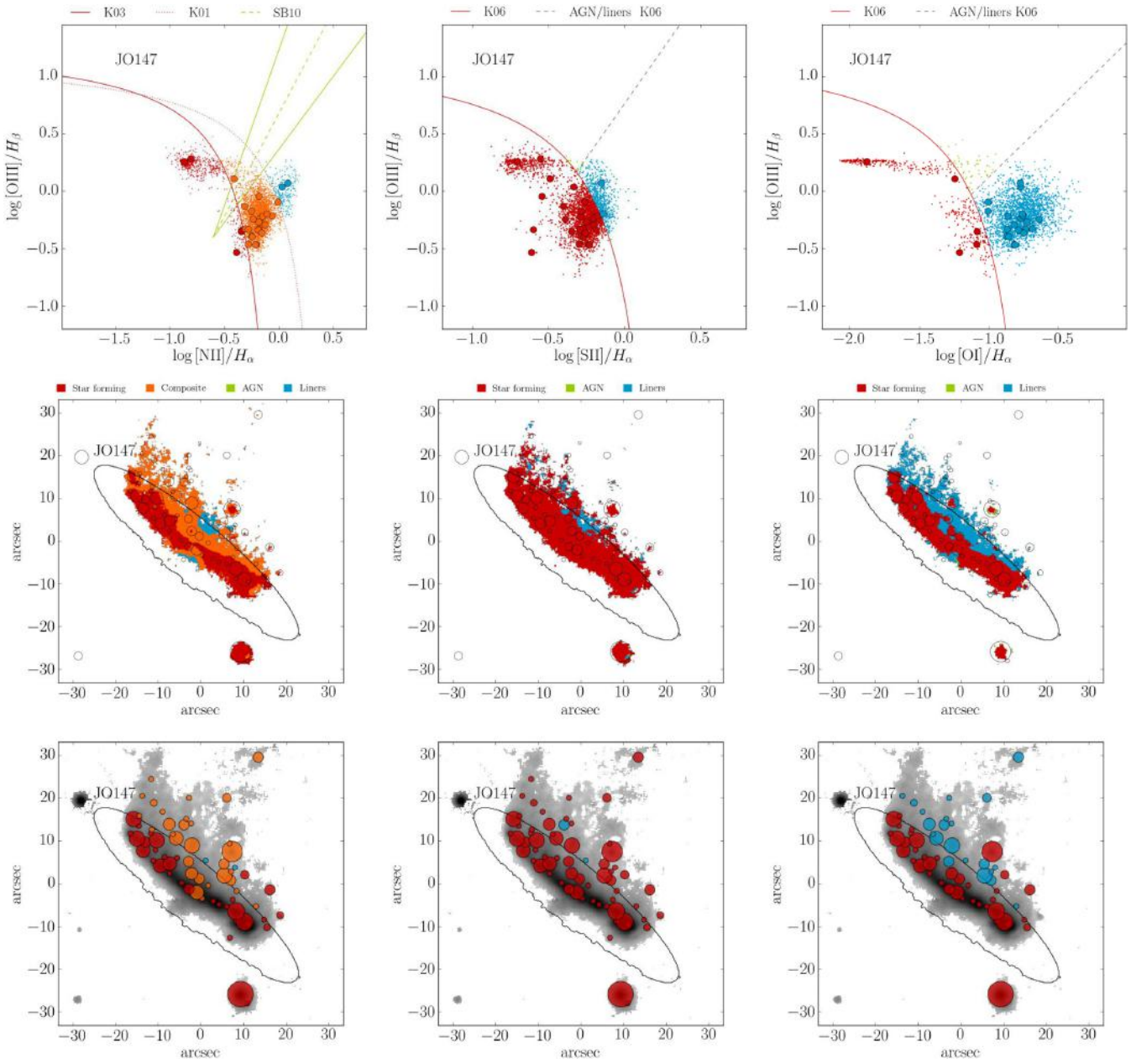

Figure 2. – *Continued*

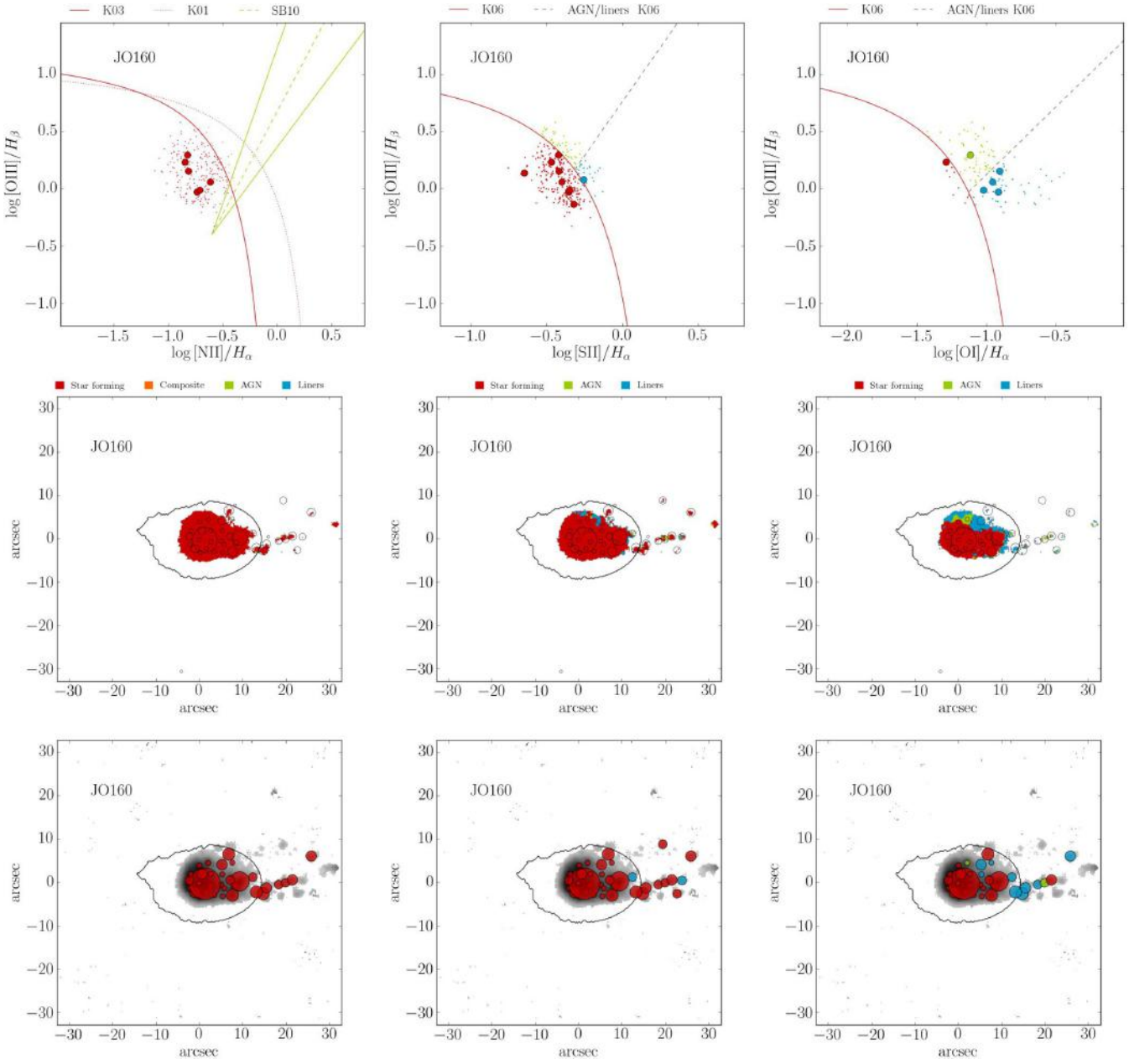

Figure 2. – *Continued*

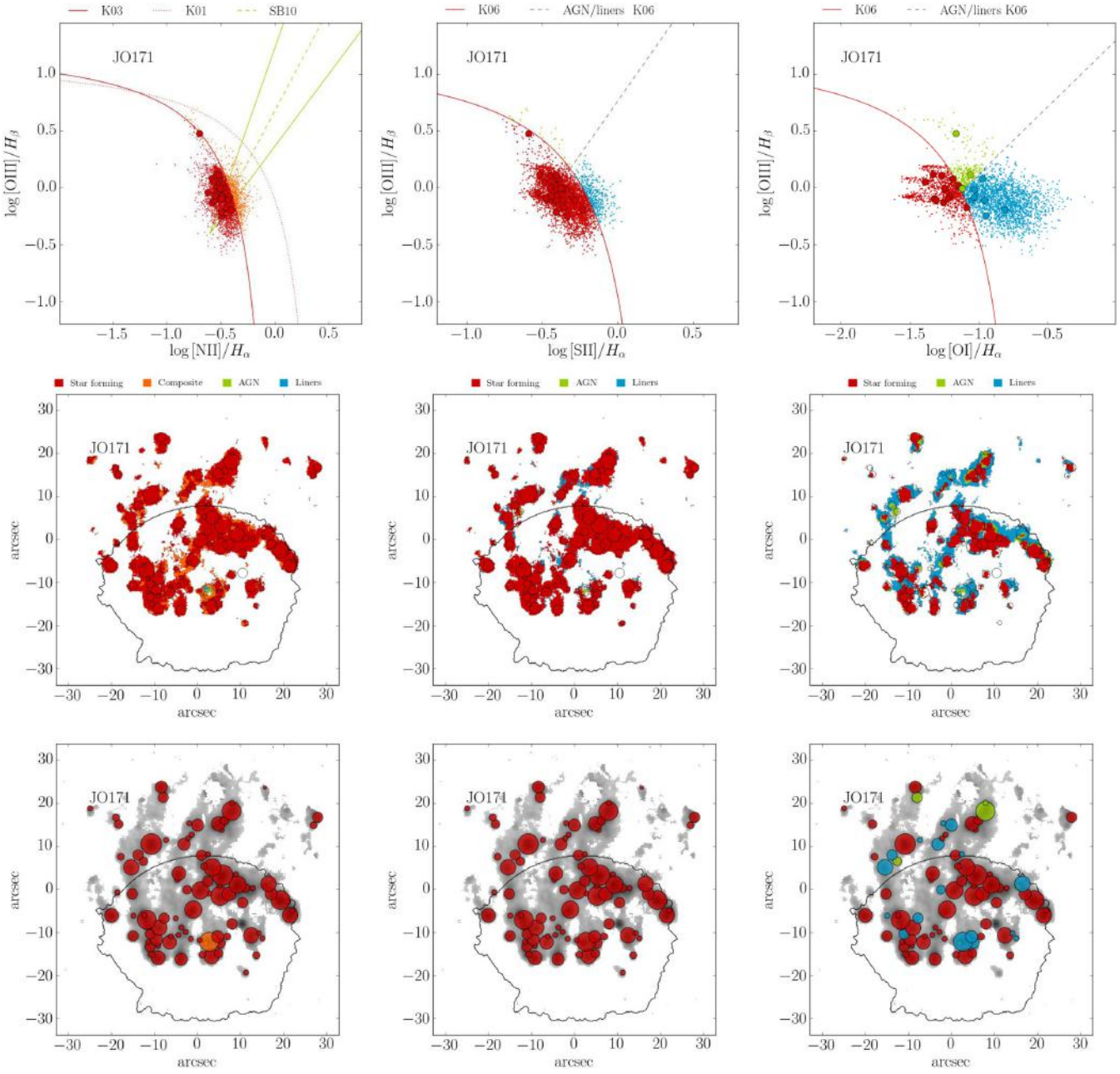

Figure 2. *– Continued*

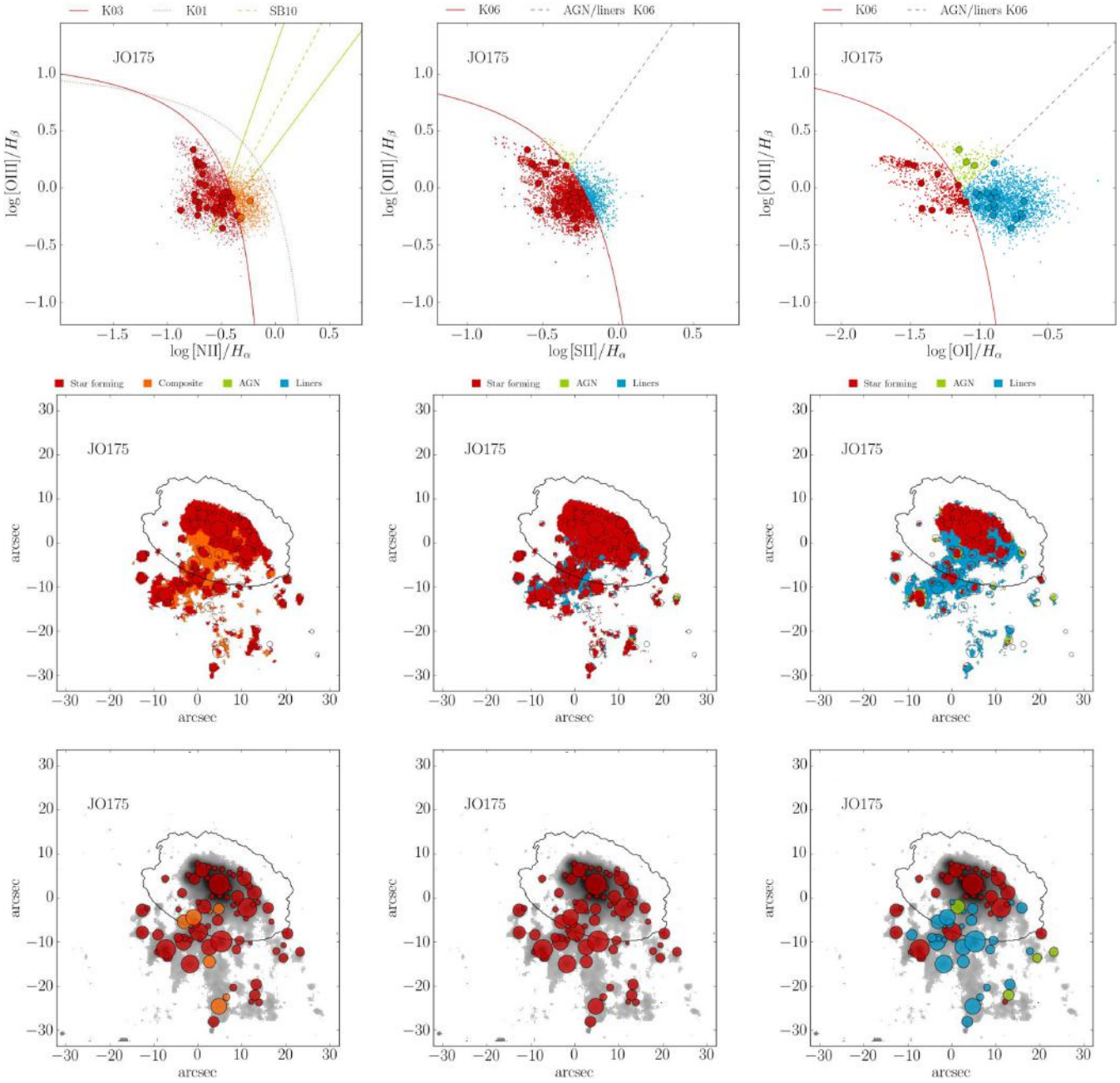

Figure 2. – *Continued*

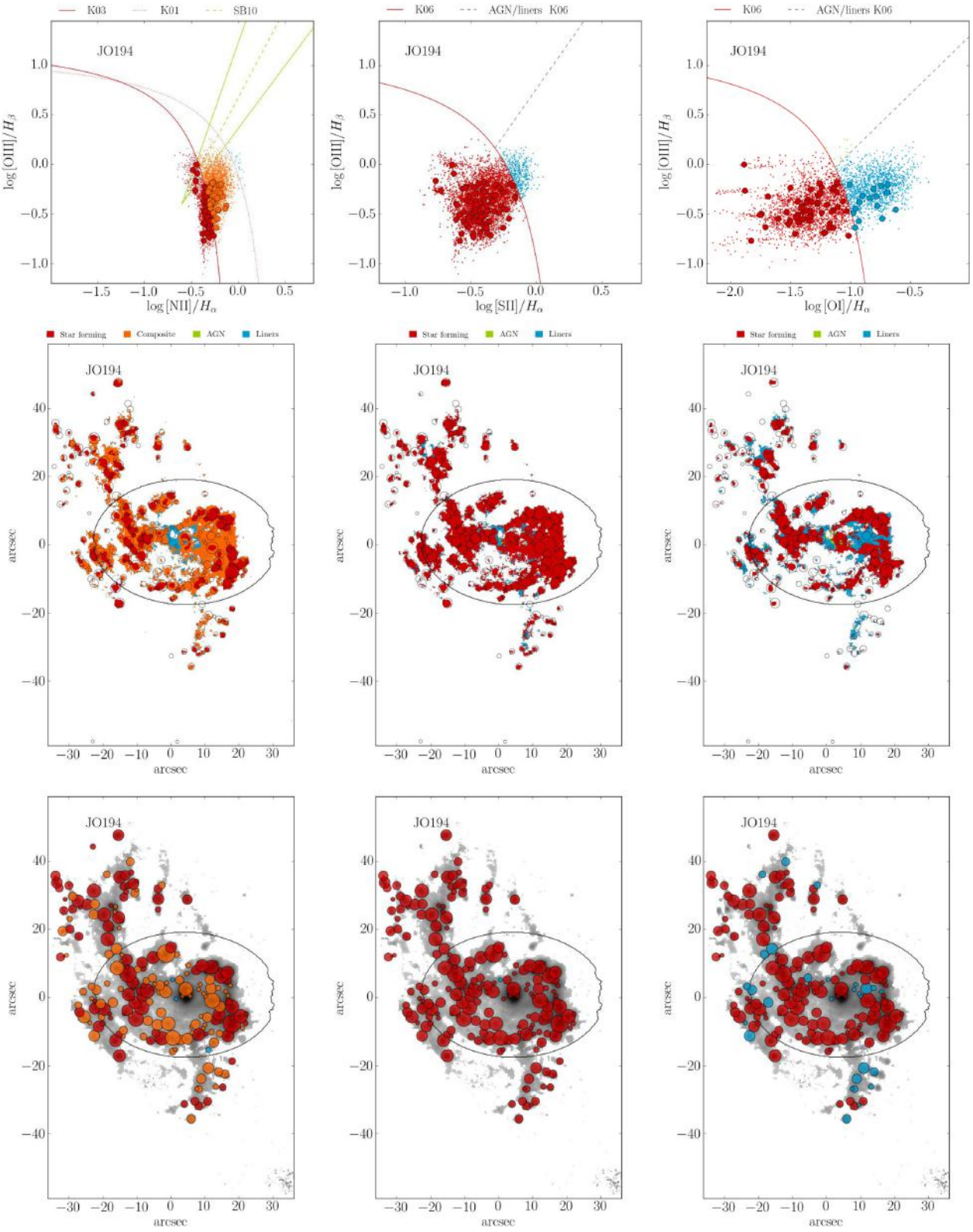

Figure 2. – *Continued*

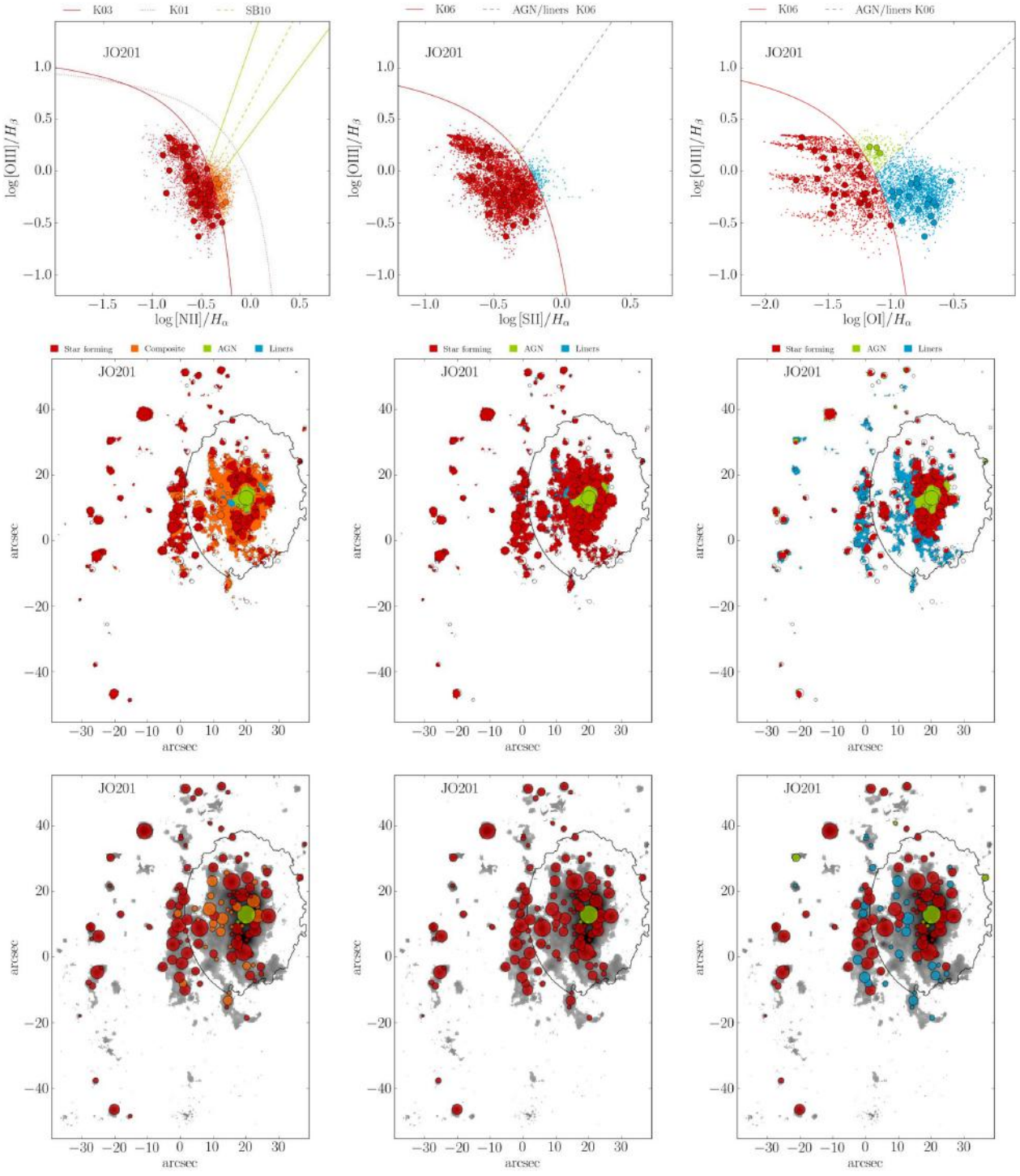

Figure 2. – *Continued*

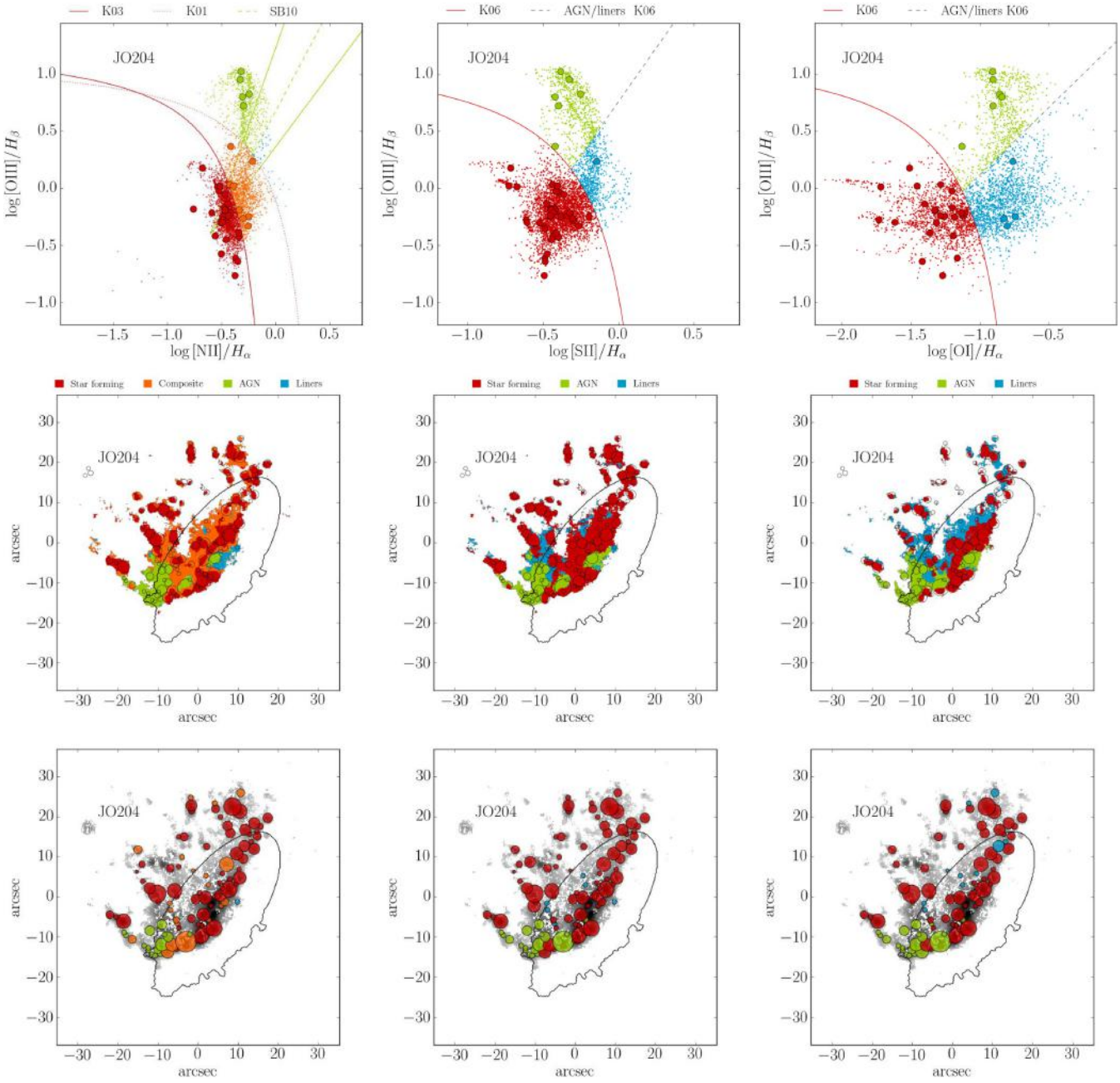

Figure 2. *– Continued*

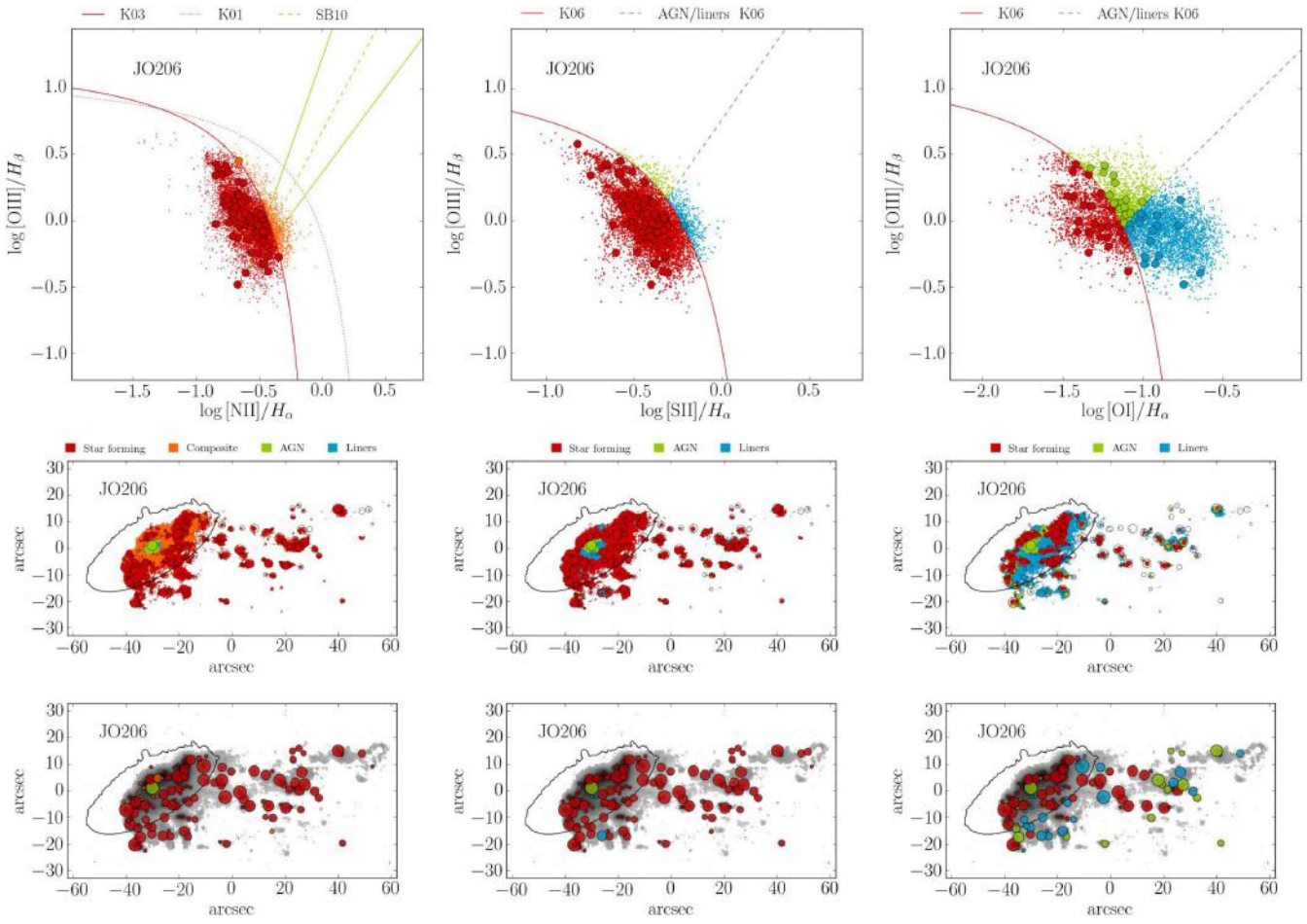

Figure 2. – *Continued*

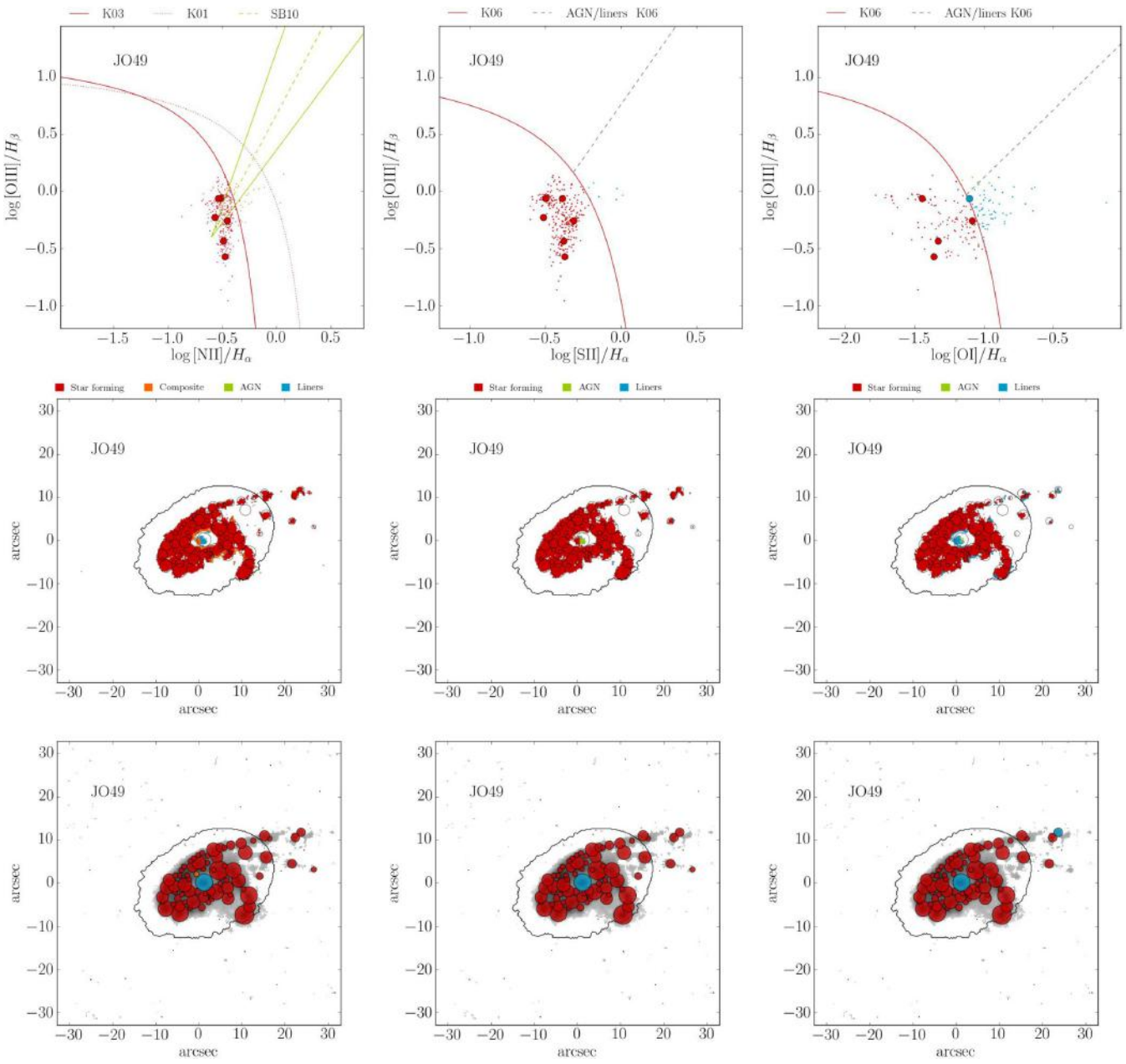

Figure 2. – *Continued*

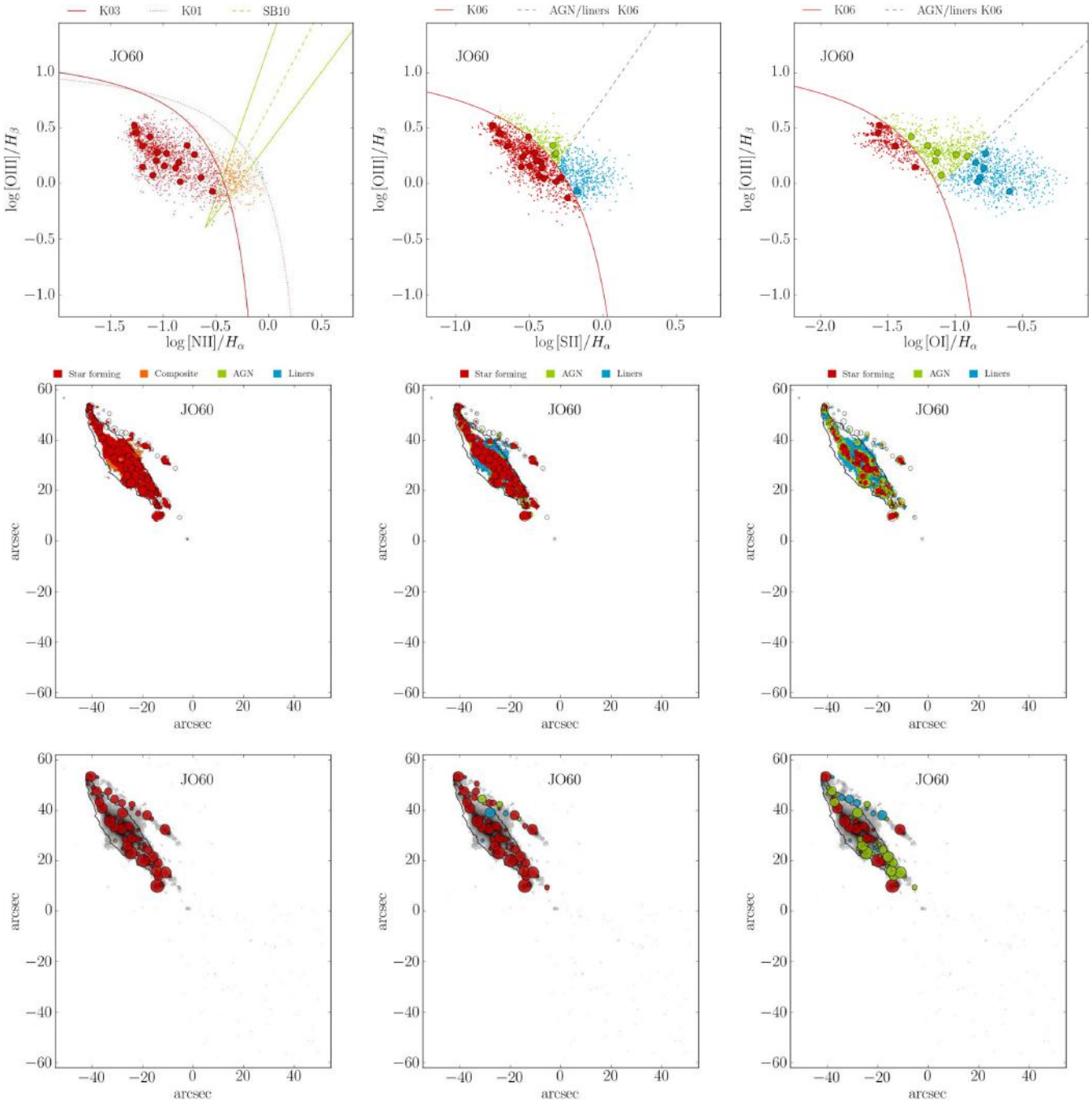

Figure 2. – *Continued*

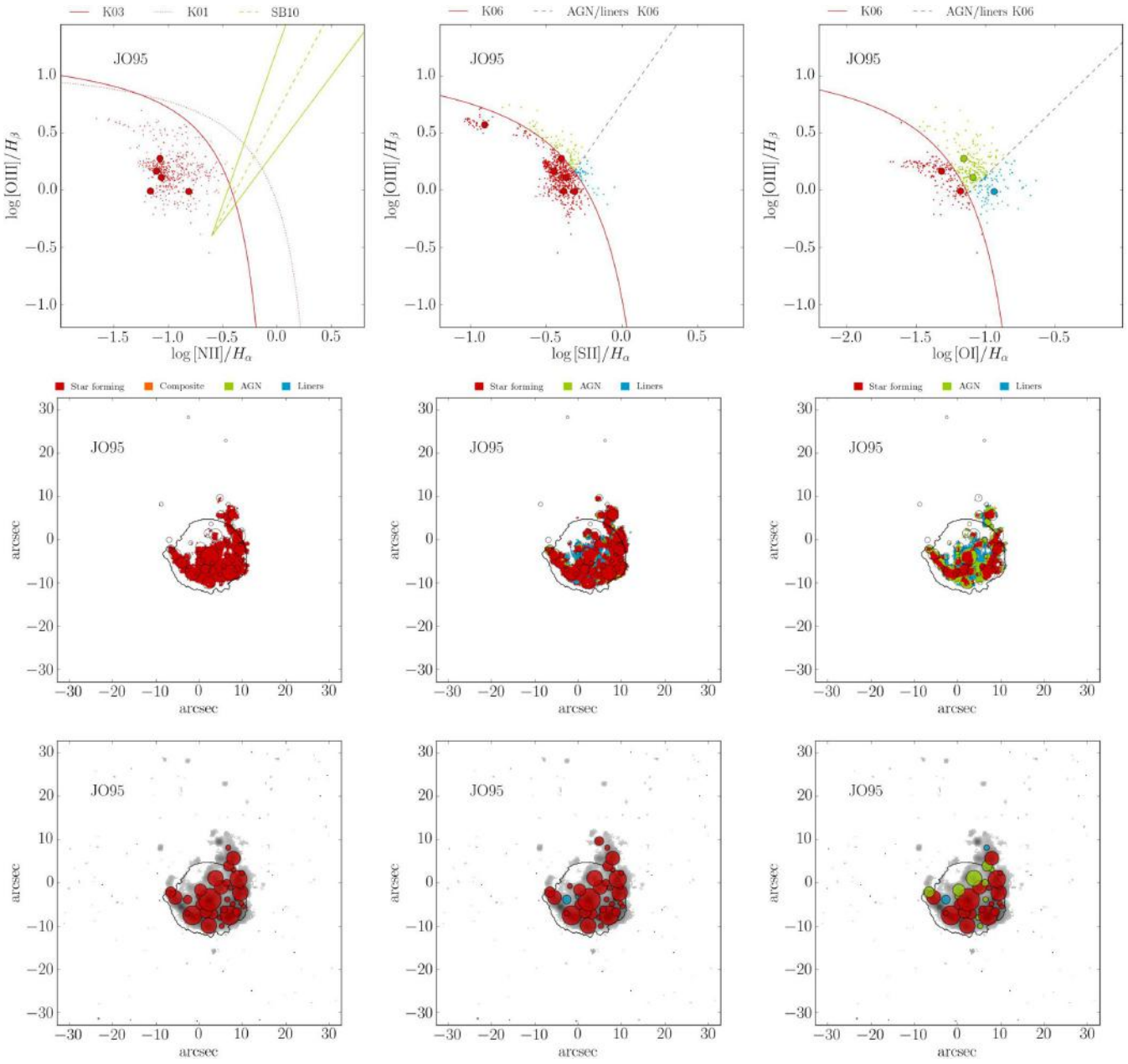

Figure 2. – *Continued*

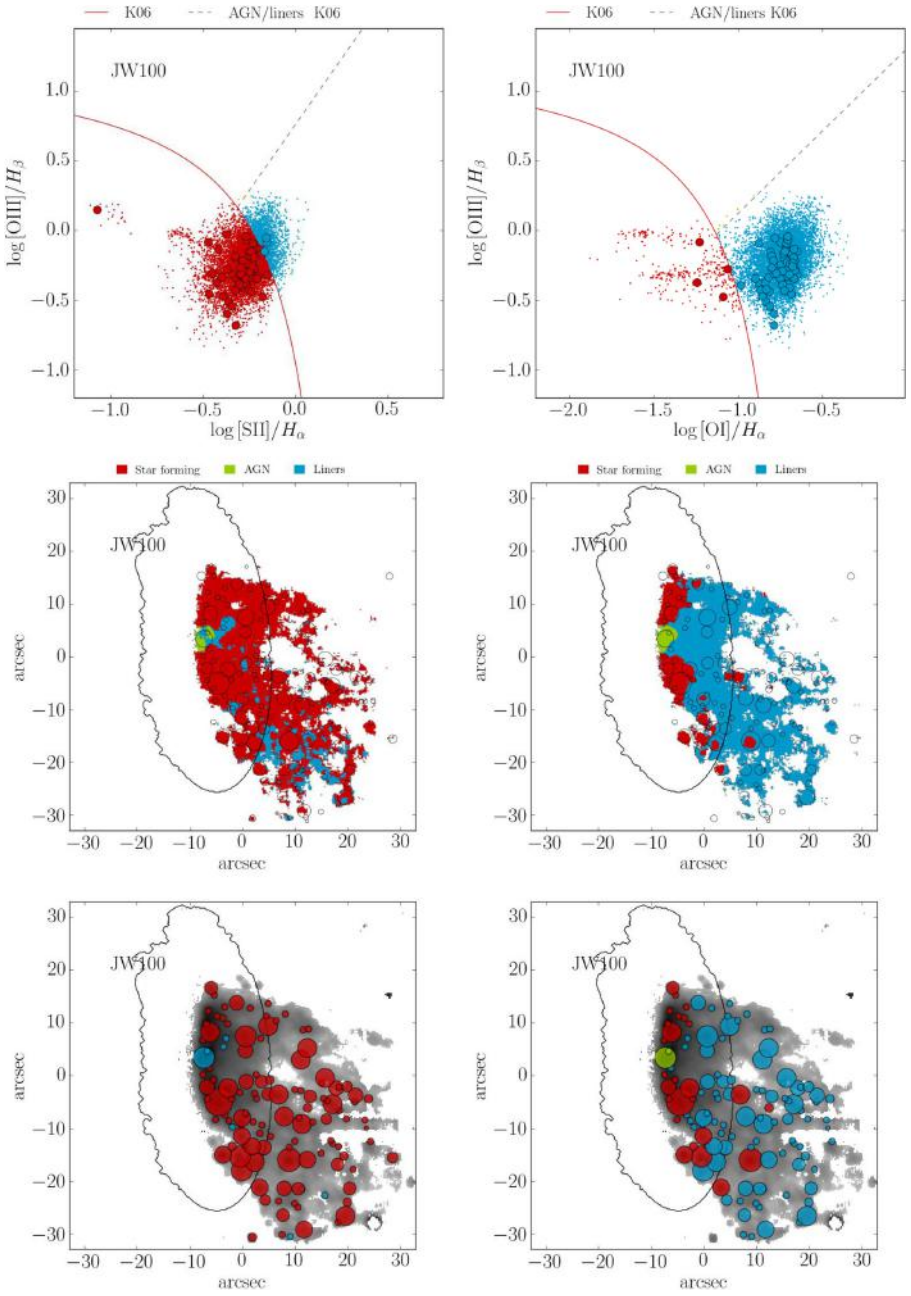

Figure 2. – *Continued*

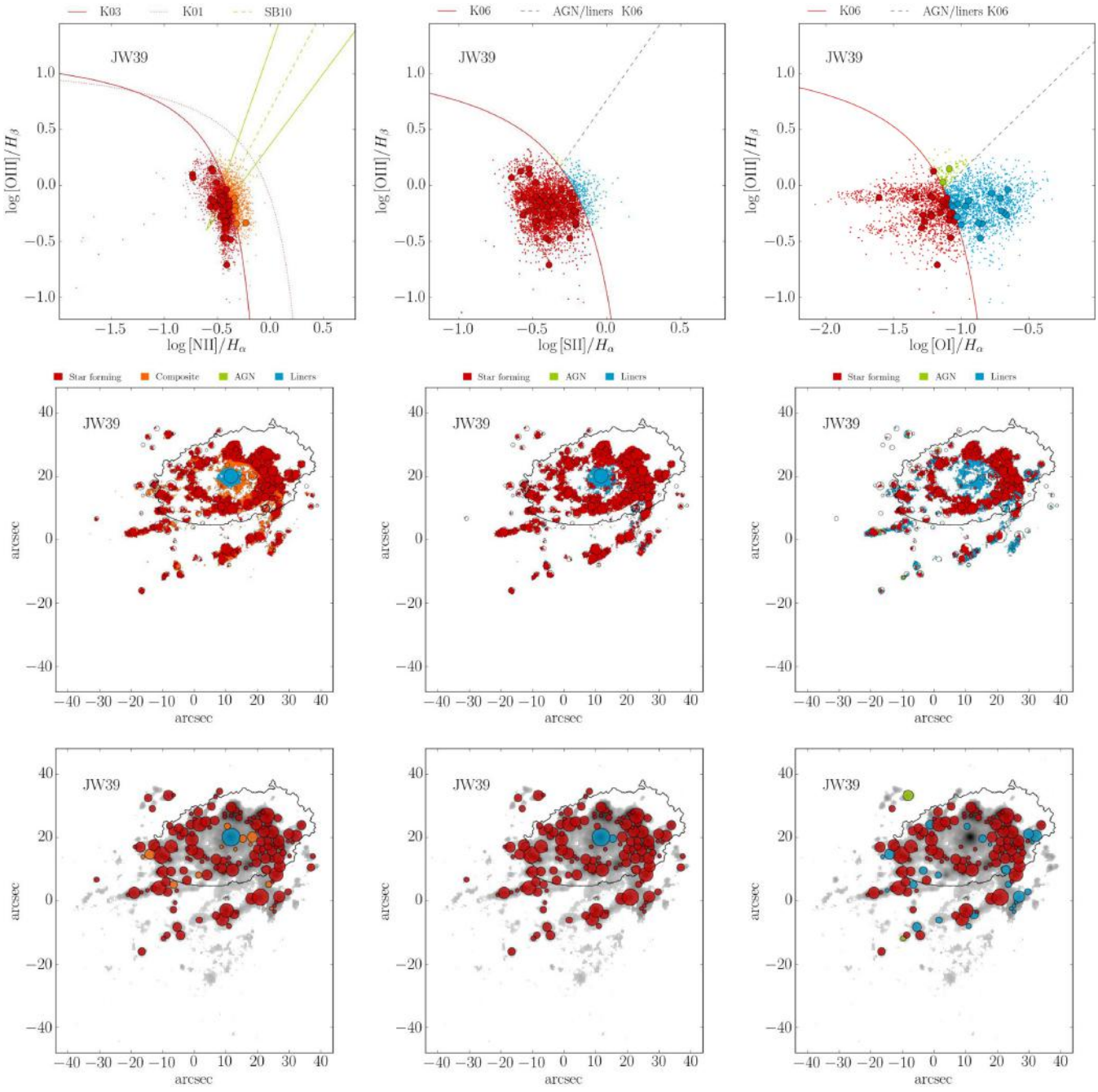

Figure 2. – *Continued*

Table 2. Percentage of Hα tail emission due to SF, Composite, AGN, and LINER according to the N II DD, and percentage of SF according to OI and S II DDs.

ID_{P16}	$SF_{N II}$	$Comp._{N II}$	$AGN_{N II}$	$LINER_{N II}$	$SF_{S II}$	SF_{OI}
JO113	99.1	0.9	0	0	72.3	19.3
JO135	52.6	17.7	20.2	9.5	68.1	35.7
JO141	93.0	7.0	0	0	83.9	47.3
JO147	59.6	37.6	0	2.8	92.6	62.7
JO160	93.9	6.1	0	0	77.7	12.8
JO171	93.8	6.2	0	0	96.7	63.0
JO175	87.7	12.3	0	0	91.2	49.7
JO194	66.1	33.8	0	0	97.8	86.1
JO201	94.1	5.9	0	0	99.2	77.3
JO204	77.2	13.8	8.9	0.2	85.4	70.2
JO206	95.6	4.4	0	0	97.1	56.6
JO49	97.2	2.7	0	0.1	99.3	77.1
JO60	96.1	3.8	0	0.1	87.8	66.9
JO95	99.7	0.3	0	0	89.1	51.6
JW100	–	–	–	–	84.4	11.4
JW39	89.2	10.8	0	0	97.1	73.5

by SF, though also the [O I] DD indicates a significant contribution from SF in the tails at the location of the brightest Hα clumps. The [O I]-LINER-like emission dominates the tails of JO147 and JW100.

Thus, the OI DD suggests a larger contribution from 'LINER/AGN' emission than the other two DDs, as previously found by e.g. Yoshida et al. (2008) and Fossati et al. (2016). This is expected in the presence of shocks (see, e.g. Rich, Kewley & Dopita 2011), which are particularly effective in triggering the [O I]/Ha ratios, compared to [N II]/Ha (Rich, Kewley & Dopita 2015). Interestingly, the LINER-like [O I] emission is mostly found in the regions *surrounding* the bright Hα clumps, and in those clumps with high gas velocity dispersion, as shown below. The exact source of [O I] excitation in the LINER regions of the tails is unknown. At their current resolution, simulations do not predict shocks in the stripped tails, and we hypothesize that thermal conduction at the boundaries where the stripped gas meets the hot ICM might play an important role.

The dominant ionization mechanism in the tails, however, is clearly star formation. According to the N II/S II/OI DDs, the median fraction of Hα luminosity in the tails powered by SF is 94(100 if SF + Composite)/91/64 per cent, ranging from galaxy to galaxy between 100/99/87 per cent and 66/68/12 (Table 2). Thus, between ∼60 per cent and 100 per cent (depending on the DD employed) of the overall tail Hα emission for which an ionization mechanism can be identified is powered by SF.

Finally, we note that all three DDs agree that two of the galaxies (JO135 and JO204) present an ionization cone from the central AGN that extends for several kpc and contributes to the ionization of gas even in the tails (see also Poggianti et al. 2017a). Nonetheless, also in these galaxies, a large fraction of the tail Hα emission appears to be powered by SF (53 per cent/68 per cent/37 per cent in JO135 and 77 per cent/85 per cent/71 per cent in JO204 from the N II/S II/OI DDs, see Table 2).

4.2 In-situ star formation in the tails

If the main source of ionization of gas in the tails are young massive stars, as shown in the previous section, it is worth asking where such stars are located.

In principle, the ionizing photons could originate from star formation in the tails or in the disc.

In the latter case, two possible situations could be envisaged: either the ionizing photons could travel a long distance from the disc before ionizing stripped neutral gas, or the gas itself could be ionized within the disc, and then stripped to large distances. Both of these situations are unrealistic, as discussed in Poggianti et al. (2017b) and below.

If the gas were ionized in the disc and then stripped, it should travel at impossibly large speeds to reach large galactocentric distances before recombining and decaying. In fact, for a gas density $n = 10\,\mathrm{cm}^{-3}$, the recombination time of hydrogen is about 10^4 yr and once recombined the decay time is negligible (Osterbrock & Ferland 2006). Thus, the gas recombination lines will be visible only for this time-scale from the moment the gas was ionized. The recombination time goes linearly with the gas density and, as we will show in the next section, the gas density in the Hα clumps is often higher than $n = 10\,\mathrm{cm}^{-3}$, implying recombination times even shorter than 10^4 yr. The maximum distance from the disc at which we observe ionized gas ranges in our galaxies between 20 and 100 kpc, meaning the gas should travel at speeds between 2×10^6 and $10^7\,\mathrm{km\,s}^{-1}$ to get there in 10^4 yr. Even for a gas density 1000 times lower ($n = 0.01\,\mathrm{cm}^{-3}$), which is unjustified based on our measurements and which would result in a recombination time-scale of 10^7 yr, the gas should move with speeds of the order of 2000–10 000 $\mathrm{km\,s}^{-1}$, which are much higher than the velocities at which these galaxies are moving within the ICM.

The possibility that the ionizing photons formed in the disc manage to escape to such large distances before encountering neutral gas to ionize is also highly unlikely. Our JVLA data shows long tails of HI neutral gas coexisting with the Hα tails (Ramatsoku et al. in prep., Deb et al. in prep.), and coexisting HI and Hα tails are present in a few other jellyfish galaxies (e.g. Consolandi et al. 2017).

The in-situ formation of new stars in the tails is therefore the most likely hypothesis, and is corroborated by other GASP results:

(1) the stripping candidates in the Poggianti et al. (2016) atlas were selected from B-band images for having unilateral debris material which indeed turned out to be the brightest Hα clumps. This B-band light stellar continuum from stars, with no significant contribution from line emission in the observed band at these redshifts, hence the visibility of these clumps in the B-band already points to the presence of blue stars in the tails.

In the same fashion, the FUV and NUV light of the O and B young stars in the clumps of the tails was directly observed with UVIT@ASTROSAT in JO201, one of the galaxies in our sample (George et al. 2018), where we found a remarkable agreeement between the SFR of individual clumps derived from the FUV and from Hα. GALEX data of several GASP jellyfishes, albeit at much lower spatial resolution, support the same scenario.

(2) In Moretti et al. (2018b) we presented APEX CO(2-1) data for four of the galaxies presented in this paper and found large amounts of molecular gas (several $10^9\,\mathrm{M}_\odot$) in the tails of these galaxies. Molecular gas was also found in the tails of three other jellyfishes in the literature (Jáchym et al. 2014, 2017; Verdugo et al. 2015). The CO observed in the tails is the smoking gun of the presence of cold, molecular gas where new stars can be born.

(3) The GASP MUSE spectra are fitted by our spectrophotometric code SINOPSIS (Fritz et al. 2017) that finds good fits to the spectra in the tails for a vigorous ongoing and recent (past few 10^8 yr) star formation. These young stars can account both for the num-

ber of ionizing photons required by the emission lines and for the observed continuum level and (blue) shape.[2]

We conclude that in-situ star formation in the tails is the cause of the photo-ionization of the SF-powered gas in the tails. The Hα clumps we identify in our galaxies are the obvious sites for such star formation, and in the next section we show they are star forming clumps, possibly composed of smaller H II regions and complexes which we cannot resolve at the 1 kpc resolution of the MUSE data.

5 THE PHYSICAL CHARACTERISTICS OF THE Hα CLUMPS

We now focus on the ionization mechanism of the Hα clumps defined in Section 3.1. The emission-line flux ratios of individual clumps displayed in Fig. 2 were estimated from the MUSE spectra integrated within each knot. The ionization mechanism could be determined for all clumps from NI and S II DD, and for ∼85 per cent of them from the OI DD. Since the cases in which the OI line is too weak to be measured are most likely to be SF regions given the location of the dividing lines in the DD, the remaining 15 per cent can be considered as star-forming.

In total, there are 521 Hα clumps in the tails of our galaxies, and 1031 inside the stellar contours of the galaxy discs. Similarly to the spaxel analysis, the NI DD analysis finds that the majority of the clumps (70 per cent) are powered by SF, and this fraction becomes 98 per cent when considering SF + Composite emission, as can be appreciated inspecting the bottom panels of each galaxy in Fig. 2. Similar conclusions are reached from the S II DD, while according to the OI DD about 60 per cent of them are powered by SF.

5.1 Gas velocity dispersion and Hα luminosity function

Fig. 3 shows the spaxel map of gas velocity dispersion for each galaxy as measured from Hα. Focusing only on the tails, there are regions of both high- and low-velocity dispersion. The high-velocity dispersion regions might be due to intrinsically dynamically 'warm' regions, or to the superposition along the line of sight of various gaseous components at different velocities. It is interesting that the two galaxies with the 'warmest' tails, JO147 and JW100 (and to a less extent JO201), are those for which the OI DD finds a strong LINER component. In these tails, the 'heated' component of the gas is clearly more prominent than in the others.

The Hα clumps in the tails (see white circles in Fig. 3) generally correspond to the regions with lowest gas velocity dispersion.

Fig. 4 presents the line ratios versus gas velocity dispersion of individual clumps in the tails. These plots show that high [N II]/Hα, [S II]/Hα and [O I]/Hα ratios (corresponding to Composite/LINER-like emission) are found in those blobs with high gas velocity dispersion ($> 50 - 70\,\mathrm{km\,s^{-1}}$), while clumps with low line ratios (star forming) have velocity dispersions typically below $50\,\mathrm{km\,s^{-1}}$. These trends are very similar to those found by Rich et al. (2011) in two luminous infrared galaxies, and are consistent with high line ratios originating when the gas is 'heated' by some other process than star formation. Thus, while clumps with low emission line ratios and low velocity dispersion have the typical characteristics of H II star-forming clumps, the fewer clumps with high ratios and high σ are probably at least partly 'heated' by other mechanisms such as thermal conduction from the ICM or turbulence due to the stripping motion, and/or are contaminated along the line of sight by the emission of more diffuse turbulent/heated gas.

The velocity dispersion distribution of the clumps is presented in Fig. 5 (panel (a)), where the black histogram indicates all the clumps in the tails of our sample galaxies. We note that the mean error on the clump σ's is about $\sim 4\,\mathrm{km\,s^{-1}}$ but uncertainties on the velocity dispersion measurements dominate for $\sigma \leq 17\,\mathrm{km\,s^{-1}}$. This, combined with the instrumental line width ($46\,\mathrm{km\,s^{-1}}$ at Hα, Section 3), prevents us from measuring reliable clump velocity dispersion values lower than $\sim 17\,\mathrm{km\,s^{-1}}$.

The median σ of all clumps in the tail is $34.9\,\mathrm{km\,s^{-1}}$ (first and third quartiles are Q1 = 23.6 and Q3 = 74.9). As already clear from Fig. 4, the tail clumps powered by SF have lower velocity dispersions than those ionized by Composite or LINER mechanisms (Fig. 5a): the median σ of SF-powered tail clumps is $27.2(Q1 = 21.0, Q3 = 39.4)\,\mathrm{km\,s^{-1}}$ according to the N II DD ($26.8(21.2 - 38.3)\,\mathrm{km\,s^{-1}}$ using the OI DD).[3] In contrast, the median for the Composite clumps is $105.9(63.9 - 155.5)\,\mathrm{km\,s^{-1}}$, while for LINERs is $74.1(61.5 - 75.1)\,\mathrm{km\,s^{-1}}$ and $87.4(49.2 - 149.8)\,\mathrm{kms^{-1}}$ for N II and OI DDs, respectively.[4]

The SF-powered clumps in the tails are therefore kinematically quite cold star-forming complexes, whose absorption- and dust-corrected Hα luminosity function is presented in Fig. 5b. As before, we present the distribution for all the clumps in the tails (solid black line), for SF-powered tail clumps (red solid NI DD, dashed OI DD), and for all the clumps in the discs (dashed black histogram).

The median clump luminosity in the tail is $4.5 \times 10^{38}\mathrm{erg\,s^{-1}}$, with the first and third quartiles being $2.5 \times 10^{38}\mathrm{erg\,s^{-1}}$ and $1.5 \times 10^{39}\mathrm{erg\,s^{-1}}$. The clump luminosities are typical of the so-called 'giant H II regions' ($L_{\mathrm{H}\alpha} = 10^{37} - 10^{39}\mathrm{erg\,s^{-1}}$, ionized by a few OB associations or massive stellar clusters, such as the Carina Nebula in our Galaxy) and 'super giant H II regions' ($L_{\mathrm{H}\alpha} > 10^{39}\mathrm{erg\,s^{-1}}$, probably ionized by multiple star clusters or super star clusters, with no analog in our Galaxy but observed in late-type galaxies and interacting galaxies, such as 30 Doradus in the Large Magellanic Cloud (Lee, Hwang & Lee 2011)). These giant and super giant H II complexes are conglomerates of many individual H II regions, corresponding to high-density condensations interconnected by a more diffuse medium (Franco et al. 2000). Our spatial resolution is limited by the seeing ($\leq 1'' = 1$kpc at the distance of our galaxies), therefore higher resolution IFU studies would be needed to probe the scales of individual H II regions within these complexes. In Section 5.5 we will discuss the issue of clump sizes in more detail.

5.2 Dust extinction and star formation rates

According to the Balmer decrement, the clumps in the tails are extincted by non-negligible amounts of dust with a median $A_V = 0.5(0.27–0.74)$ mag, see Fig. 5c. This median value remains very similar if we select only SF-powered clumps. Only 9 per cent of the tail clumps have an $A_V > 1$ mag. The extinction in the tail clumps is lower on average than the one in the clumps that are in the galaxy discs, whose median is 0.74 mag and where 28 per cent of the clumps have an $A_V > 1$ mag.

[2]We note that the continuum gas emission is not included in spectrophotometric models, and this remains a source of uncertainty.

[3]These medians should be lower limits but also close approximations of the true values for the limitations on velocity dispersion measurements discussed in the text.

[4]For completeness, for AGN-powered clumps in the tails the median is $35.5(32.0 - 55.6)\,\mathrm{km\,s^{-1}}$ and $24.0(19.2 - 32.4)\,\mathrm{km\,s^{-1}}$.

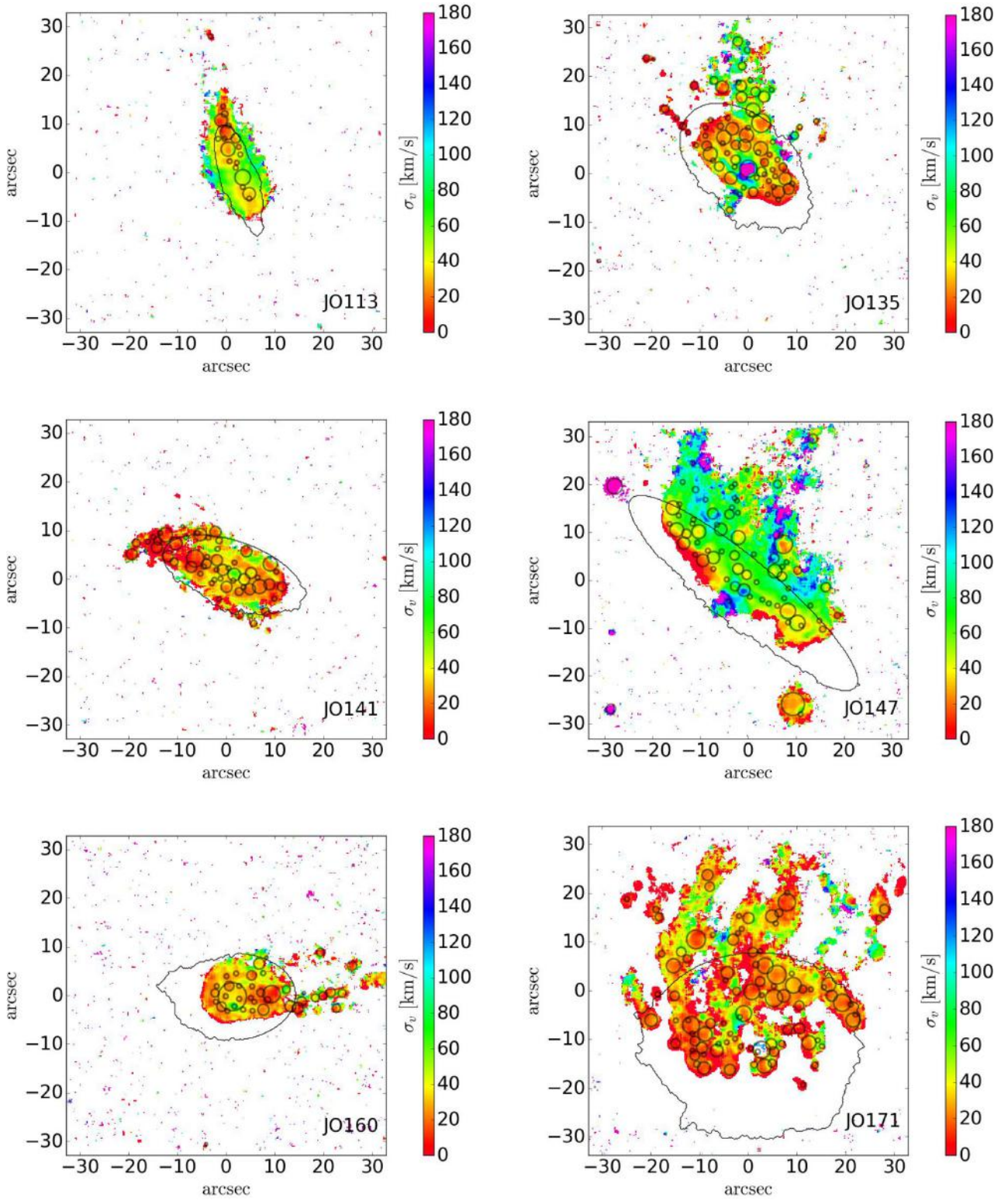

Figure 3. Gas velocity dispersion maps. Grey circles are the Hα clumps.

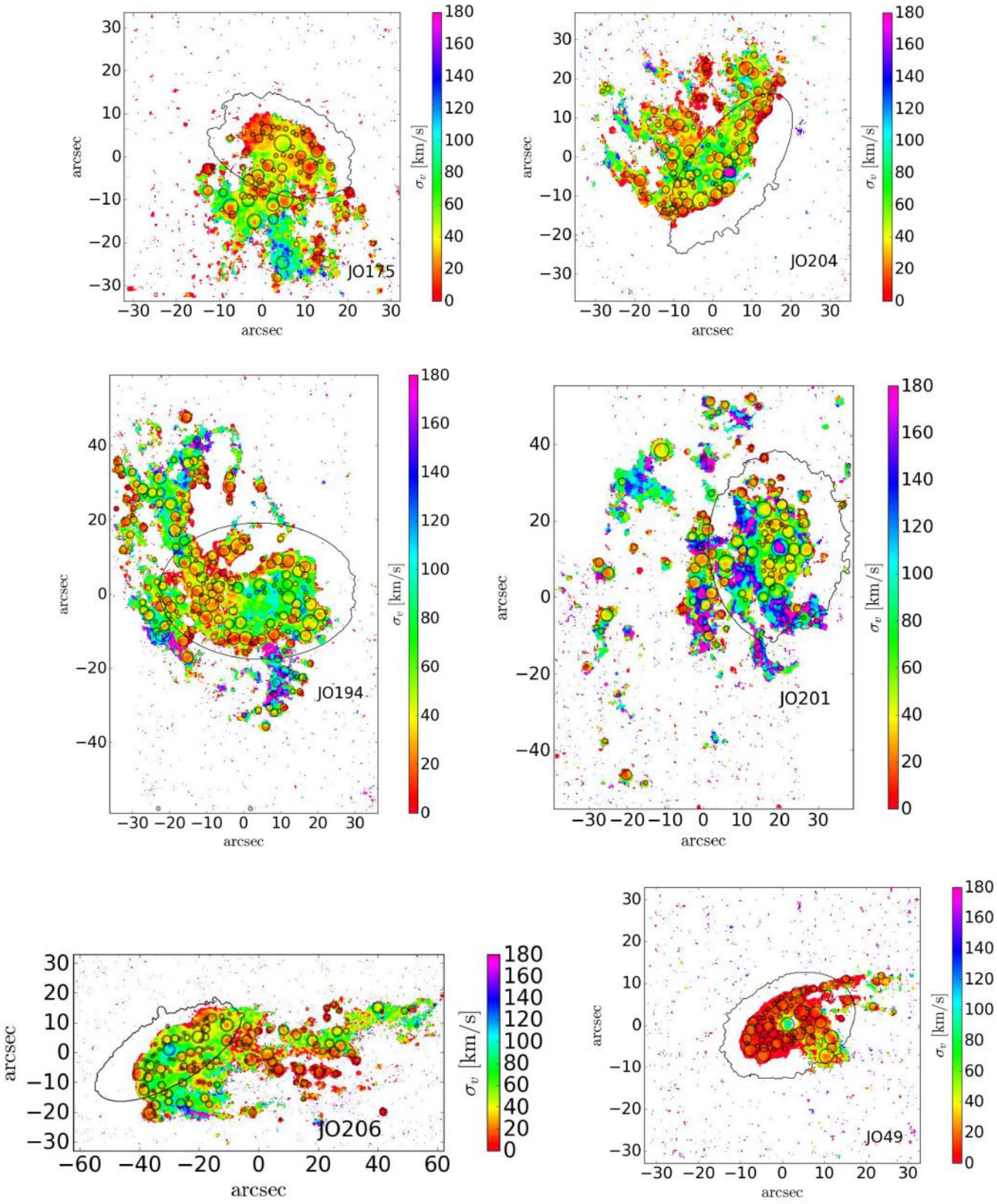

Figure 3. *– Continued*

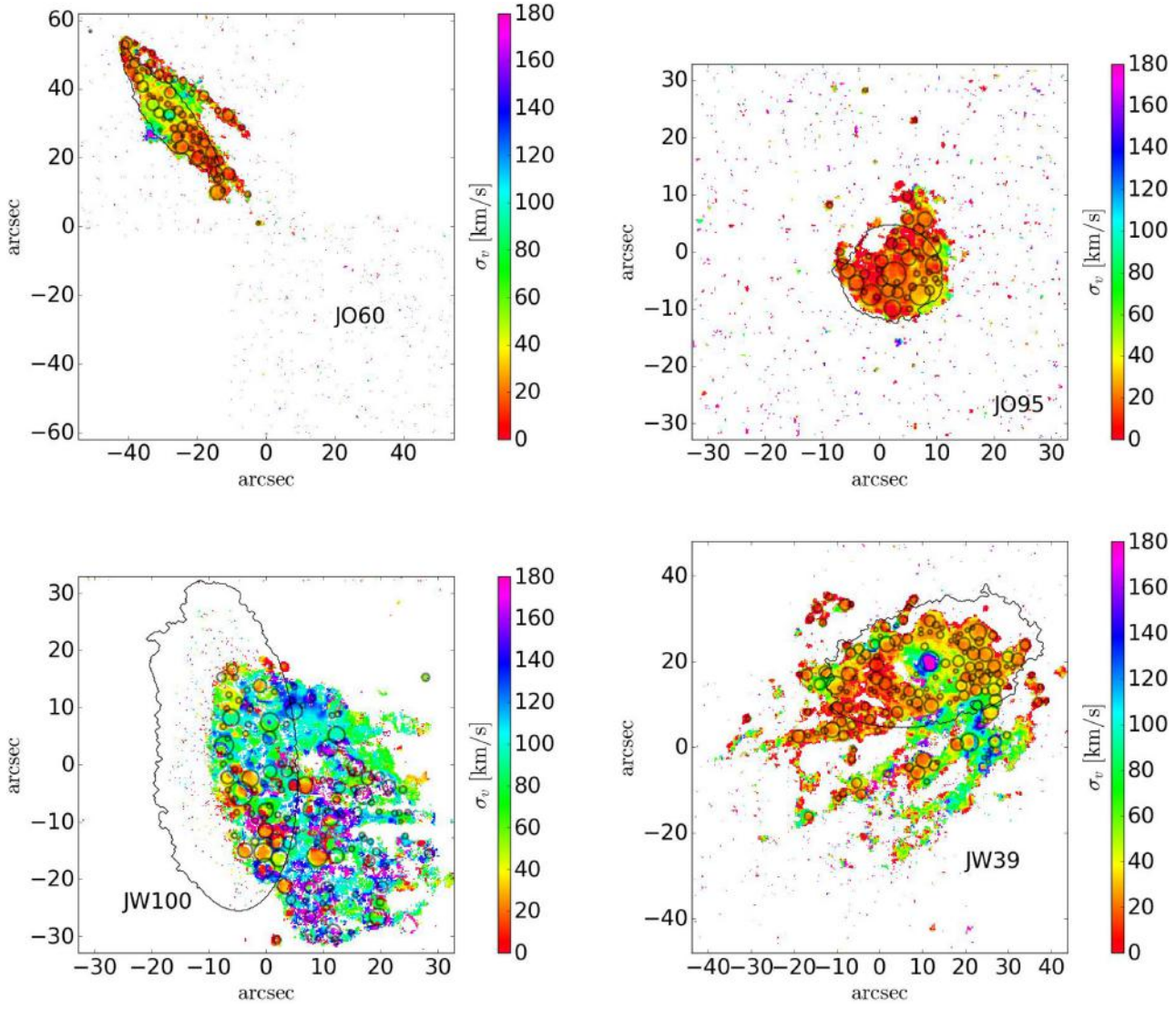

Figure 3. – *Continued*

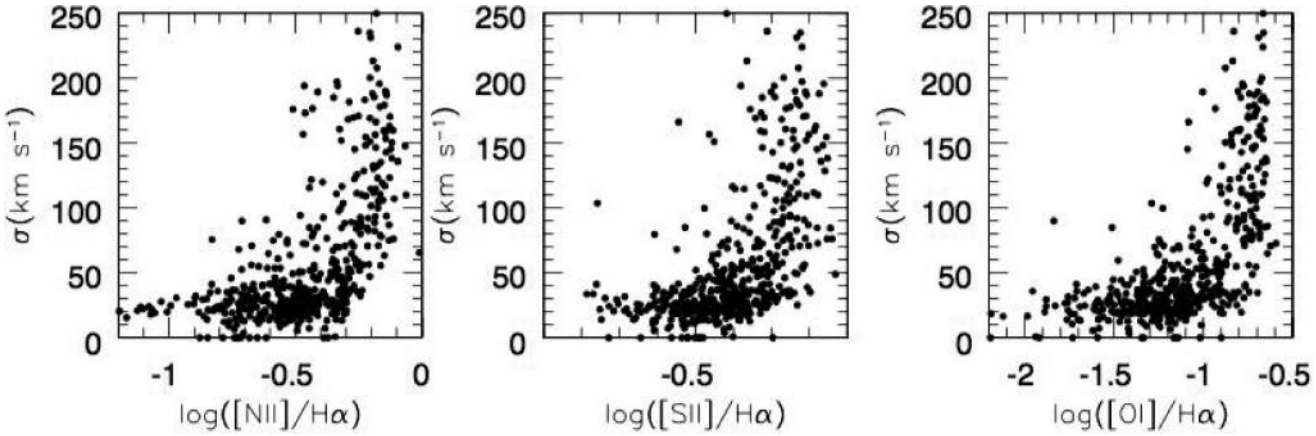

Figure 4. Plot of line ratio versus gas velocity dispersion for individual clumps in the tails.

Having corrected the Hα emission for the extinction by dust, we derive the SFR distribution of individual clumps (Fig. 5d). While the median SFR of clumps within the disc is 0.012 $M_\odot$ yr^{-1} (Q1 = 0.004, Q3 = 0.037), the one of the star-forming tail clumps is 0.003 (Q1-Q3 = 0.001–0.008) $M_\odot$ yr^{-1} (0.005 using OI DD). Almost all the tail clumps have SFR lower than 0.1 $M_\odot$ yr^{-1}, while in the disc they can form up to 1 solar mass/year.

IMF stochasticity in regions of low SFR leads to underestimate on average the SFR measured from the Hα emission. For an observed Hα SFR of $\sim 10^{-3}$ $M_\odot$ yr^{-1} this effect is about an order of magnitude assuming a Kroupa IMF and a constant SFR over 500 Myr (da Silva, Fumagalli & Krumholz 2012, 2014). A detailed analysis of the effects of stochasticity on our SFR estimates is beyond the scope of this paper and will be treated in a following work. Until then, the SFR values quoted in this paper can be considered lower limits.

5.3 Gas and SFR densities

It is interesting to estimate the ionized gas densities within the clumps.

The gas density can be measured only for about half of the clumps in the tails (276 out of 521) because for the others the ratio of the two [S II] lines falls out of the usable range (see Section 3). This is true also if we consider only clumps powered by SF (e.g. 122/205 for OI DD). Thus, the values quoted below refer to the clumps for which the Proxauf et al. (2014) calibration can be used, while an estimate for the other half of the clumps cannot be obtained.

The median n_e in tail star-forming clumps for which a measurement is feasible is 51.5 cm^{-3}, with a large spread (see solid lines in Fig. 4e) with Q1 = 21 and Q3 = 108 cm^{-3}. The gas density distribution of clumps in the disc (where an estimate of n_e cannot be obtained for 1/3 of the clumps) has a different shape and is surprisingly skewed towards lower densities than the tail distribution, though it covers a similar range of values, as can be seen in Fig. 5e, with a median of 35.6 cm^{-3}.

In Fig. 6 we show the density map of clumps in JO206, as an illustrative case of the general trends. The clumps for which the density cannot be estimated are grey circles, and the higher average density in the tails compared to the disc is also evident. However, given the incompleteness of the n_e measurements especially in the tails, the significant overlaps of different clumps especially in the disc, and the spatial resolution limit which might result in including into each clump also the lower density surroundings, a definitive understanding of the differences between the disc and tail clump densities must await higher resolution data. What our analysis conclusively shows, however, is that dense gaseous clumps are found in the tails.

Turning to the SFR density (herafter SFRD) inside the clumps, this cannot be simply estimated from the total SFR in the clump and the clump area because of the likely overestimation of the clump sizes (see Section 5.5). The SFRD spaxel maps (Fig. 7) give us a view of the variation of the SFRD from clump-to-clump, and between clumps and regions of diffuse emission. The SFRD typically reaches logarithmic values between −2.5 and −1.5 $M_\odot$ yr^{-1} kpc^{-2} in the central spaxels of the brightest clumps in the tails, while higher SFRD can be reached in the clumps inside the discs.

5.4 Gas and stellar masses

The distribution of ionized gas masses of the clumps (Fig. 5f) shows that in the tails they range between $\sim 10^3$ and $\sim 10^7 M_\odot$ (in the disc up to 10^8), with a median for star-forming clumps equal to $\sim 4 \times 10^4$ in the tails and 2×10^5 in the disc.[5]

While inside the disc stellar contours the clump stellar masses are derived from the fits that use SSPs of all ages (because the discs contain also old stars in the line of sight of any H II region), for the stellar mass estimates of clumps in the tails SINOPSIS has been run placing an upper limit to the age of the stellar populations (6×10^8 yr), in order to avoid having very low levels of unrealistically old stars in the tails, whose light contribution is insignificant, but whose integrated stellar mass can result in overestimating the stellar mass. We have tested that the stellar masses of the tail clumps do not change appreciably varying the upper age limit between a few 10^7 and 10^9 yr, therefore this measurement can be considered stable. In the following, it is important to keep in mind that while the stellar masses of tail clumps are indeed the masses of stars associated with the H II complexes observed, the stellar masses of clumps in the discs are strongly influenced by the total stellar (old and young stars) mass density variations within the discs, and cannot be considered representative of the population of young stars in the H II complexes. In a sense, tail clump masses are 'true stellar masses' of the clumps, while disc clump masses are 'projected stellar masses' inflated by the underlying old stellar populations.

[5] Since these values are computed from the gas density, the number of clumps for which the gas mass can be estimated is the same as the number of clumps with n_e measurements.

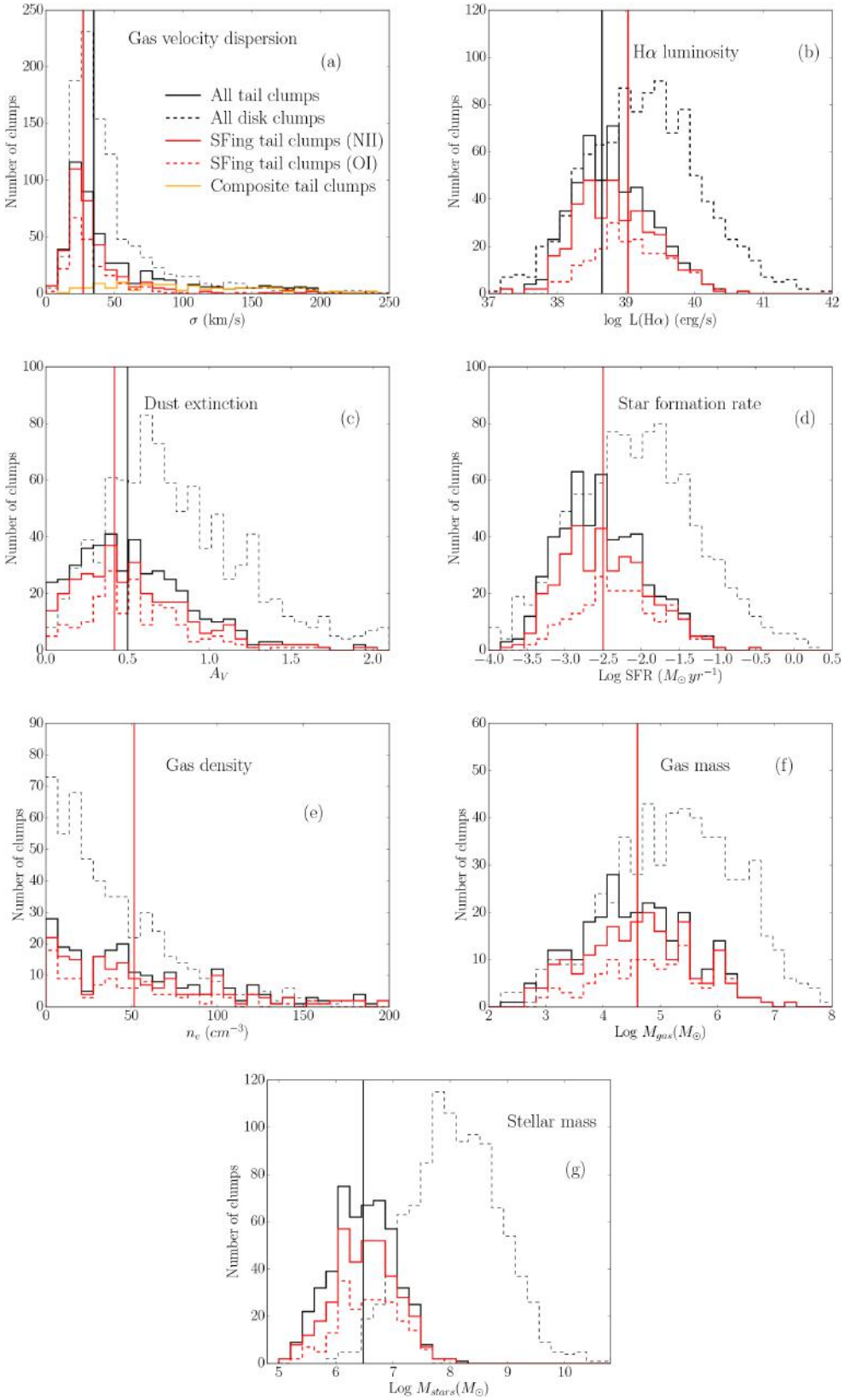

Figure 5. Clump physical properties. Panel a): Gaseous velocity dispersion distribution of clumps in the tails. Solid black: all clumps. Red solid: SF from N II DD. Red dashed: SF from OI DD. Orange: Composite from N II DD. Dashed black: clumps in the galaxy discs. Panel b): Hα clump luminosity distribution in tails (solid histograms) and discs (dashed histograms). Panel c): Dust extinction A_V. Panel d): SFR distribution. Panel e) Gas density distribution. Panel f): Gas mass. Panel g): Stellar mass. Vertical lines indicate median values.

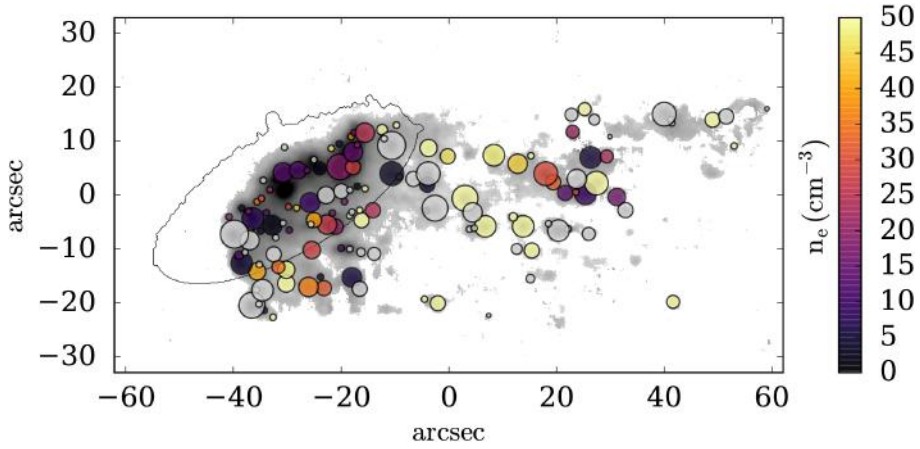

Figure 6. Gas density of the star-forming + composite clumps of an illustrative case, JO206. Grey-filled circles are the clumps for which n_e cannot be measured (see text). The underlying grey map shows the Hα map.

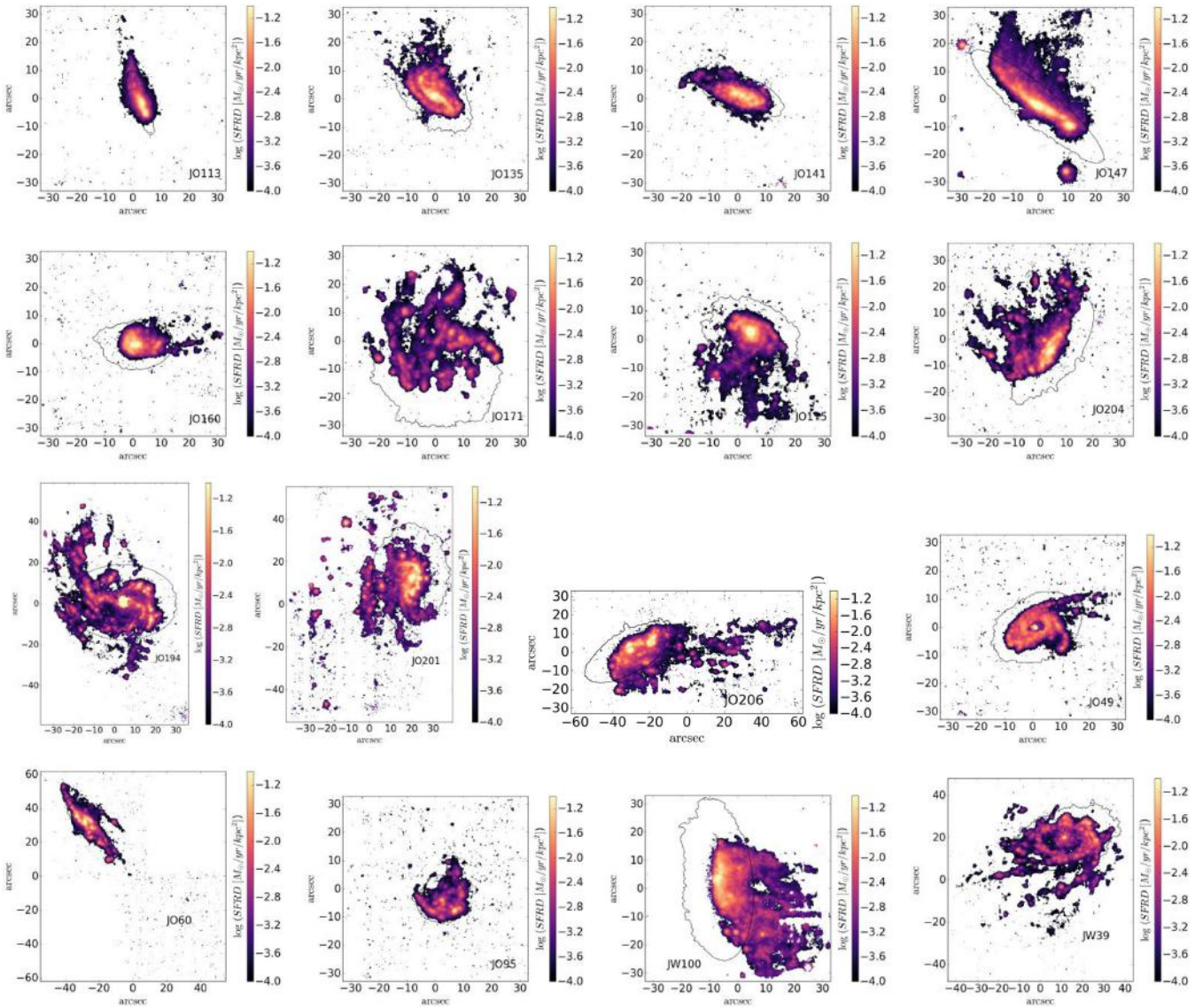

Figure 7. Star formation rate density maps.

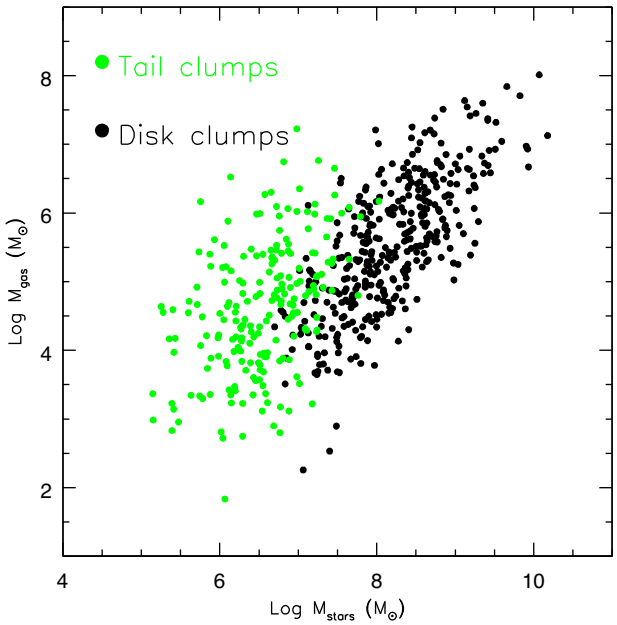

Figure 8. Relation between ionized gas mass and stellar mass of star-forming clumps in the tails (green) and 'projected stellar masses' of clumps in the discs (black, see text).

The stellar masses of the clumps in the tails range between 10^5 and 3×10^7 $M_\odot$, with a median of 3×10^6 $M_\odot$ (Fig. 5g). In the discs, the 'projected stellar masses' (old + young stars) range between $3 \times 10^6 - 3 \times 10^9$, with a median 10^8. Comparing the stellar masses of clumps in the tails and discs is obviously not meaningful, for the reasons explained above, but we do plot the 'projected stellar masses' of disc clumps in Fig. 5g for completeness. As for the SFR, the assumption of a standard Chabrier (2003) IMF introduces a large uncertainty in the stellar mass estimates that should be kept in mind.

The fate of the stars formed in the tails will be discussed in a subsequent paper of this series discussing their contribution to the intra-cluster light (Gullieuszik et al. in prep.). Tail stars, especially those closer to the disc, may remain bound to the parent galaxy, and fall back onto it contributing to the thick disc or the bulge (Abramson et al. 2011; Kapferer et al. 2009). If unbound, they will remain an intracluster population of 'stripped baryonic dwarfs', as predicted by some simulations of ram-pressure stripping (Kapferer et al. 2008). If the tail stellar clumps have indeed stellar masses between 10^5 and 10^7 $M_\odot$, depending on their sizes they could resemble Ultra Compact Dwarf Galaxies (UCD) and Globular Clusters (GC) for effective radii below 100 pc, or Dwarf Spheroidals (dSph) for sizes greater than 100 pc (Norris et al. 2014), except that they would be dark matter free. In the next section, we will present rough size estimates (Fig. 10, median 160pc) of the H II gaseous clumps, which are likely upper limits to the sizes of the stellar clumps embedded within them. Based on this, we suggest that most likely the stellar clumps we see forming in the stripped tails may contribute to the abundant population of UCDs and GCs observed in galaxy clusters (Hilker, Infante & Richtler 1999; Drinkwater et al. 2000; Wittmann et al. 2016), or even the population of Ultra Diffuse Galaxies (UDGs) depending on their subsequent interactions with the cluster potential and other galaxies, for example via harassment (Conselice 2018). Predicting the metallicities and the subsequent dynamical history of these stellar clumps within the cluster is beyond the scope of this paper and will be pursued in future studies.

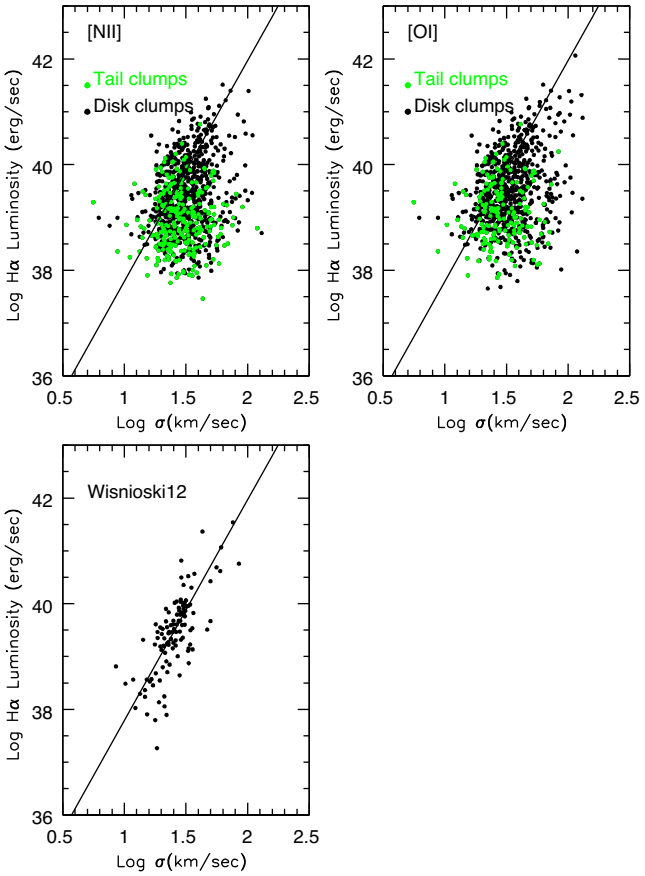

Figure 9. Top. Hα luminosity versus velocity dispersion of the star-forming clumps in the tails (green) and in the discs (black). These are all clumps classified as star-forming by the N II DD (top left panel) and the OI DD (top right panel). Solid lines represent the scaling relation by Wisnioski et al. (2012). Only points with reliable velocity dispersion estimates are plotted (errors on σ >0 and excluding the worst error quartile). Bottom. Same as top, but plotted are H II regions in low-z galaxies from Wisnioski et al. (2012). The line is the same in all panels.

Finally, we compare the gas masses and stellar masses of tail clumps in Fig. 8 (green points), and notice a broad correlation, with stellar masses typically one or two orders of magnitude higher than the corresponding ionized gas masses. A similar, but offsetted correlation exists between the gas masses and the 'projected stellar mass' of clumps in discs. In the next section, we will investigate the correlation between the SFR and the gas and stellar masses of the clumps.

5.5 Clump scaling relations

Star-forming regions both at low- and high-z have been found to follow scaling relations linking their physical characteristics, such as sizes, gas velocity dispersion and Hα luminosity (Terlevich & Melnick 1981; Larson 1981; Gallagher & Hunter 1983; Monreal-Ibero et al. 2007).

Wisnioski et al. (2012) showed that the gas velocity dispersions of star-forming clumps are unaffected by spatial resolution effects and that the Hα luminosities are quite insensitive to the chosen clump radius, being consistent when measured within isophotal or core radii (see Section 3.1). Based on the robustness of the measurements of these two quantities, in Fig. 9 we inspect the σ-L(Hα) relation of our clumps, and contrast it with the Wisnioski

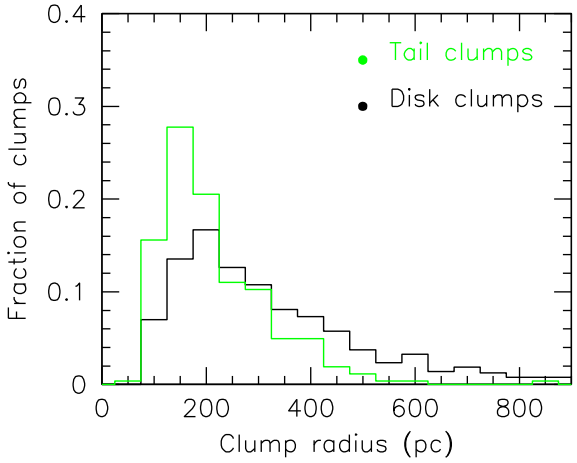

Figure 10. Distribution of clump core radii inferred from the relation between Hα luminosity and size. Green: tail clumps. Black: disc clumps.

et al. relation (solid line) and their low-z data points (bottom panel in Fig. 9). The paucity of points at σ below $\sim$17 km s^{-1} in Fig. 9 is due to the intrinsic limit to our velocity dispersion measurements discussed previously. Apart from this limit, it is remarkable that both the clumps in the disc and those in the tails seem to broadly follow the scaling relations of normal star-forming galaxies at low-z, albeit with the presence in GASP galaxies of a subset of clumps which seem to deviate from such relation due to their low Hα or, more likely, increased velocity dispersion.

This result gives us confidence that normal-galaxy scaling relations might be used to have a very rough estimate of the true physical sizes of our star-forming clumps, below the limit imposed by the seeing. Adopting the relation between Hα luminosity and size for low redshift spirals, irregulars and starburst galaxies (Equation (6) in Wisnioski et al. 2012), we estimate the core radii of our clumps. The distribution of estimated sizes is presented in Fig. 10. The typical expected core radii range from 100 to 400 per cent in the tails (median 160 per cent), and extend up to 600 per cent in the discs (median 220 pc). These values are smaller than the 1 kpc corresponding to the seeing limit. For comparison, the median size in the Wisnioski et al. sample is 150 per cent.

Finally, we show that the GASP clumps follow very clear correlations between clump SFR and clump stellar mass, and between SFR and gas mass (Fig. 11). In the SFR–stellar mass relation, there is an offset between tail clumps and disc clumps, which is due to the inflated 'projected stellar mass' of clumps in the disc. This offset disappears in the SFR–gas mass relation, which is a tight sequence followed both in the tails and in the discs: more massive gas clumps form a larger amount of stars per unit time. Both the SFR and the ionized gas mass depend linearly on the Hα luminosity (Section 3), thus a correlation is expected. However, the gas mass depends also on the gas density, therefore the width of the correlation is related to the spread in gas density from clump-to-clump. What is most striking is the fact that star-forming clumps in the tails and in the discs follow the exact same relation with a similar scatter, indicating that the range of physical conditions is not too different.

6 DIFFUSE EMISSION

The star-forming clumps are not the only location with Hα emission in the tails. Regions of diffuse emission with lower Hα surface brightness are present in the interclump areas of the tentacles of all our galaxies. In the following, we will name 'diffuse emission' the Hα component that has not been assigned to any clump.

The diffuse component accounts for a significant fraction of the Hα luminosities in the tails, on average 50 per cent, ranging between 30 and 80 per cent (see Table 3).

There is a very strong anticorrelation between the fraction of Hα luminosity that is in the diffuse component and the total SFR in the tail (Fig. 12): the higher the SFR, the lower the diffuse fraction. Hence, tails whose Hα emission is dominated by clumps can reach much higher SFR levels, or, conversely, tails with high levels of Hα emission/SFR are dominated by the star-forming clumps.

In most of our galaxies, according to the N II DD the dominant ionization mechanism of the diffuse emission in the tail is star formation, or a combination of SF and Composite, as summarized in Table 3. SF + Composite emission accounts for at least 98 per cent of the tail emission in all galaxies, except in JO135 and JO204 that, as discussed above, have AGN ionization cones extending in the tail, and in JO147 where there is a 10 per cent LINER component.

Considering instead only the pure SF component (no Composite) in the N II DD, this dominates ($\geq$ 80 per cent) the emission in the tails of 9 of our galaxies (JO113, JO141, JO160, JO171, JO201, JO206, JO49, JO95, JW39). SF still accounts for more than the half of the tail emission in JO175 and JO60 (66 per cent and 58 per cent, respectively), and only for about 20–30 per cent in JO135 (29 per cent), JO204 (36 per cent) and JO194 (21 per cent). Finally, as previously mentioned, JO147 and JW100 have tails dominated by a Composite emission, also in the diffuse component. We note that the S II DD generally agrees closely with N II and not with OI (see Fig. 2), but also that since the gas in the tails, on average, has lower metallicities than the one in the disc (e.g. Poggianti et al. 2017b, Gullieuszik et al. 2017), the N II DD could be affected by metallicity variations (Kewley et al. 2001).

As, although to a lesser extent, it was the case for the overall tail emission and for the tail clumps (Sections 4.1 and 5), especially for the diffuse emission the OI DD indicates a much stronger contribution from ionization mechanisms different from SF than the N II DD (see Table 3). In addition to JW100 and JO147, whose N II and OI estimates agree remarkably well indicating that the tail emission is dominated by Composite/'LINER-like' processes, in all the other galaxies the OI fraction of tail diffuse emission powered by SF ranges from 2 per cent to 63 per cent, with a median of 18 per cent. Four of our galaxies have a particularly strong SF component according to the OI DD ($\sim$40–60 per cent in JO206, JO49, JW39, and JO194). Understanding the origin of the significant differences we observe from one galaxy to another will be an important step in grasping the physics at work, and will be the subject of future GASP investigations.

The OI DD is capable to highlight a contribution from other physical processes which are particularly relevant for the origin of the diffuse emission. Thermal conduction from the surrounding hot ICM and turbulence are promising candidates in this respect. It is also worth noting that the spaxels for which the OI DD classification can be derived are a subset of the spaxels where N II DD can be used, due to the lower signal in the OI line, and where the OI is weak and a classification cannot be derived is most probably a SF-powered region. Thus, the OI DD might give a more biased view of the results in favor of non-SF mechanisms. The differences between the N II and S II vs. OI results are probably indicating that the diffuse emission originates partly from star formation and partly from turbulence/thermal conduction, in a relative proportion which we cannot ascertain from the current analysis.

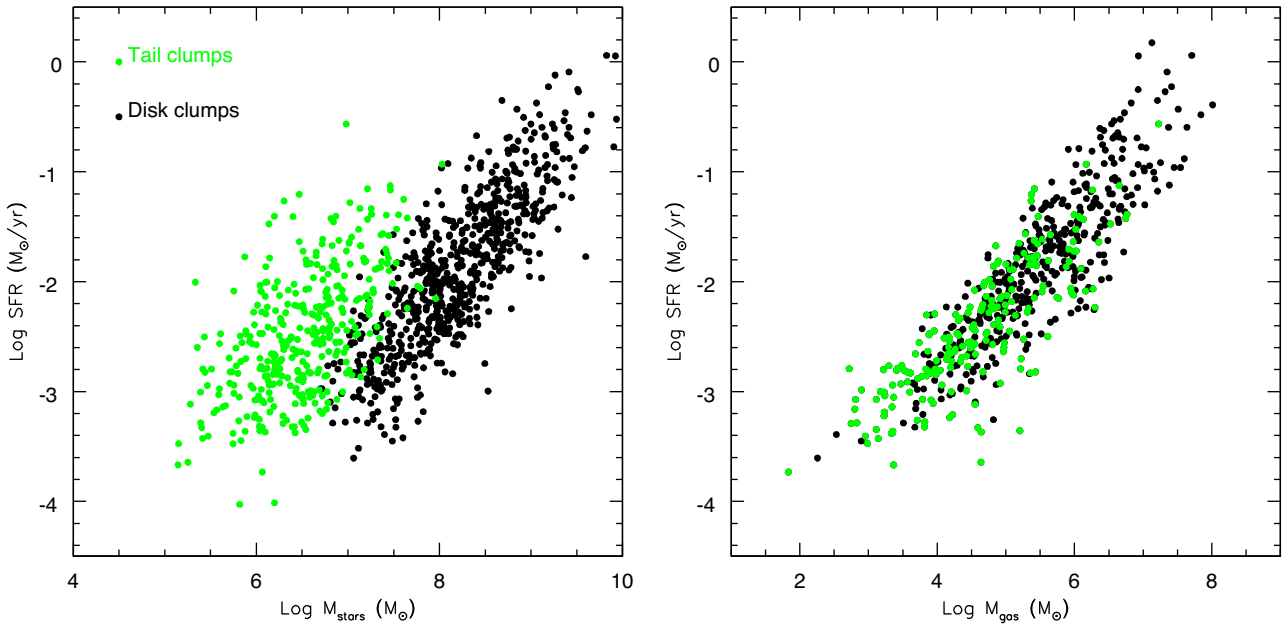

Figure 11. SFR-stellar mass (left) and SFR-gas mass (right) relations of clumps in the tails (green) and in the discs (black).

Table 3. Diffuse versus clump emission and SFR. (1) Galaxy name; (2) Fraction of tail $L_{H\alpha}$ that is diffuse; (3) SFR in the tail ($M_\odot$ yr^{-1}). (4) Fraction of tail SFR that is diffuse; (5) % of diffuse emission powered by SF; (6) % of diffuse emission powered by SF + Composite; (7) Total SFR (disc + tail, $M_\odot$ yr^{-1}); (8) % of SFR that is the tail. All the columns until column (8) included refer to the N II DD. Column (9) presents the % of tail diffuse emission powered by SF for OI DD.

(1)	(2)	(3)	(4)	(5)	(6)	(7)	(8)	(9)
JO113	0.74	0.035	0.44	0.98	1.00	1.70	0.020	0.04
JO135	0.58	0.019	0.06	0.29	0.49	1.94	0.010	0.15
JO141	0.55	0.037	0.10	0.98	1.00	2.51	0.015	–
JO147	0.39	0.204	0.22	0.03	0.91	4.64	0.044	0.04
JO160	0.79	0.007	0.23	0.99	1.00	1.94	0.004	0.12
JO171	0.39	0.351	0.22	0.81	1.00	1.63	0.216	0.19
JO175	0.49	0.110	0.19	0.66	1.00	2.48	0.044	0.08
JO194	0.28	0.436	0.13	0.21	1.00	8.31	0.052	0.63
JO201	0.30	1.002	0.11	0.80	1.00	6.06	0.165	0.14
JO204	0.39	0.221	0.13	0.36	0.71	1.68	0.130	0.18
JO206	0.39	0.511	0.19	0.90	1.00	5.32	0.100	0.39
JO49	0.77	0.010	0.13	0.93	0.99	1.38	0.007	0.48
JO60	0.35	0.185	0.08	0.58	0.99	4.47	0.041	0.02
JO95	0.62	0.018	0.13	0.98	1.00	0.37	0.048	0.22
JW100	0.52	0.806	0.46	0.003	0.98	4.02	0.200	0.009
JW39	0.38	0.387	0.15	0.78	1.00	3.31	0.117	0.55

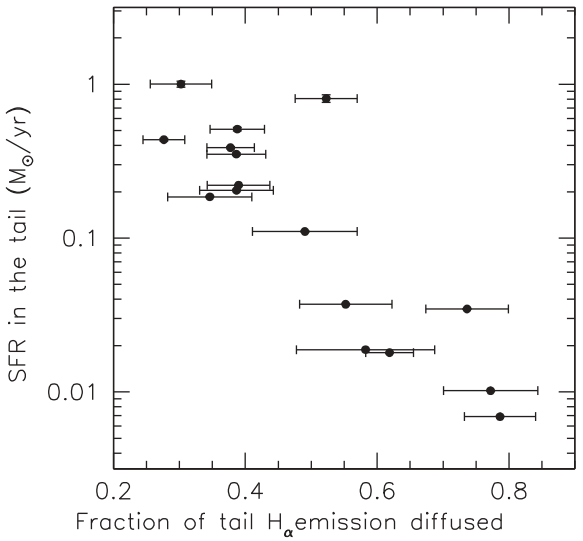

Figure 12. Total SFR in the tail (*Y* axis, solar masses per year, clumps + diffuse) versus fraction of tail Hα emission that is in the diffuse component for the 16 galaxies in our sample.

Regardless of the DD employed, SF is present in tails, though is not sufficient to explain all the ionized emission. Where are the stellar sources ionizing the gas that produces the diffuse emission? While in the case of the clumps there are several lines of evidence demonstrating it is in-situ star formation within the clumps, the diffuse tail emission might originate either from low levels of in-situ star formation (a more widespread population of lower luminosity H II regions), or from ionizing photons escaping the H II regions within the clumps and going to ionize more diffuse neutral gas located where no stars have managed to form. This would resemble what happens in the disc of normal star-forming galaxies, where the escape fraction is negligible over the whole galaxy but is significant at the scales of single H II regions and complexes (Oey & Kennicutt 1997; Wofford, Leitherer & Salzer 2013; Hernandez et al. 2018). Given also the low density of the gas giving rise to the diffuse component, leakage of ionizing photons from the tail clumps is a plausible origin for the diffuse emission.

Under the assumption that the diffuse gas is ionized locally by photons escaping the H II regions, the average escape fraction in a tail can be estimated from the MUSE data, and it is equal to the per cent of SFR in the tail that is in the diffuse component (see Table 3), In fact, the escape fraction is the ratio between the number of ionizing photons that escape the H II regions (which is proportional to the SFR-powered Hα luminosity, hence the SFR, in the diffuse component in the tails) and the total number of ionizing photons (proportional to the total SFR in the tails). Using the N II DD,

this escape fraction in our sample would be on average 18 per cent (median 15 per cent) and ranges between 6 and 46 per cent, in broad agreement with the values found in individual star-forming regions (Oey & Kennicutt 1998; Relaño, Peimbert & Beckman 2002). This is probably an upper limit to the intrinsic escape fraction, due both to the assumptions and the differences between the N II and OI estimates. This hypothesis cannot be confirmed based on the existing data, and requires the comparison of our Hα maps with high resolution, deep ultraviolet imaging as might be obtained with e.g. HST.

7 STAR FORMATION RATES IN THE TAILS AND THE DISCS

The total SFR (disc + tails) of each of our galaxies is presented in Table 3 together with the fraction of total SFR that is in the tail.

Our jellyfishes form in total between 1.5 and 6 $M_\odot\,yr^{-1}$, with two outliers being JO194 with 8.3 $M_\odot\,yr^{-1}$ and JO95 with $\sim$0.4 $M_\odot\,yr^{-1}$ (Table 3). The location of GASP galaxies in the SFR-stellar mass diagram is the subject of a separate paper (Vulcani et al. 2018c).

The fraction of total SFR that takes place in the tail can vary significantly, between less than 1 per cent and more than 20 per cent of the total activity, as shown in Table 3. The SFR occurring in the tail represents 10 to 20 per cent of the total in 6 of our galaxies (JO206, JW39, JO204, JO201, JW100, and JO171), which are those with the longest tails, as it is reasonable to expect. In another 5 galaxies the tail SFR is about 4–5 per cent of the total (JO60, JO147, JO175, JO95, JO194), while for the remaining 5 galaxies it is at the 1–2 per cent level (JO113, JO141, JO135, JO49, JO160).

Most of the SFR in the tails is concentrated in the clumps, typically >80 per cent.[6] The only two galaxies with significantly lower fractions ($\sim$55 per cent) are JO113 and JW100, in which the diffuse emission is more prominent.

8 DISCUSSION

8.1 The frequency of tail star formation and previous observational results

Ongoing star formation is present in the tails of all our sample galaxies. In a future work we investigate how the star formation in the tails depends on the galaxy properties, the cluster properties and the galaxy position in the velocity-clustercentric distance diagram using the full GASP sample (Gullieuszik et al. in prep.).

Since the GASP targets were sourced from the Poggianti et al. (2016) atlas, they all have visible unilateral debris in the B-band images, therefore they might be expected to host SF in the tails by selection. Hence, our results do not rule out the possibility that stripping can occur without extraplanar star formation. Moreover, the sample presented in this paper consists of galaxies that are all subject to strong ram pressure stripping, and with long tails of extraplanar Hα emitting gas. Galaxies in a more advanced stage of stripping (i.e. truncated gaseous discs with gas left only in the centre, or fully stripped galaxies devoid of any gas) were excluded in this work, and require a separate analysis to assess whether they have had an Hα tail phase at some point and whether stellar-only extraplanar clumps are still visible.

[6]We note that the fraction of tail SFR that is in the clumps is equal to 1 minus column (4) in Table 3.

It is probable, as also expected from simulations, that SF in the tails occurs only during the phase of peak-stripping, and when ram pressure is sufficiently strong to produce significant gaseous tails. Gaseous tails can be observed at various wavelengths, detecting gas in different phases: a) with HI observations detecting stripped neutral hydrogen, b) in X-ray detecting gas heated at the interface between the hot ICM and the cold stripped ISM, c) observing Hα emission with narrow-band or IFU observations to probe the ionized/excited gas phase, and d) with CO observations to study the molecular gas. How frequently tails of various gas phases coexist is still unknown, as it is unknown how this frequency depends on the ICM conditions and the galaxy properties. Studies of the HI (Kenney, van Gorkom & Vollmer 2004; Crowl et al. 2005; Oosterloo & van Gorkom 2005; Chung et al. 2007; Abramson et al. 2011) or X-ray tails (Sun & Vikhlinin 2005; Sun et al. 2006, 2010) require additional information to inform us about the ongoing or past tail SF, that can come from Hα or UV data.

The great majority of previous UV or Hα studies of stripped tails find evidence for ongoing or recent SF in the tails. The most solid evidence can be obtained with IFU or spectroscopic studies, that allow us not only to detect Hα emission but also to assess the ionization mechanism from multiple line ratios. Before GASP there were three well-studied such cases:

(a) ESO137-001 in Abell 3627 (stellar mass $\sim$5–8 $\times$ 10^9 $M_\odot$) was the first one which it was unambiguously shown to host star-forming H II regions in the cold stripped ISM by Sun et al. (2010) using Gemini spectra (see also Sun, Donahue & Voit 2007), as confirmed by MUSE subsequent studies (Fumagalli et al. 2014) that found these H II regions form in low- velocity dispersion gas (25–50 km s^{-1}) and have quite typical line ratios, densities, temperatures and metallicities, suggesting they are formed in situ within the tails (Fossati et al. 2016). Large amounts of molecular gas were found in the tail of this galaxy by Jáchym et al. (2014).

(b) UGC6697 (10^{10} $M_\odot$) in Abell 1367, a tidally interacting system in which ram pressure stripping may have been enhanced by the encounter. After several multiwavelength campaigns detecting radio continuum, Hα and X-ray tails (Gavazzi et al. 1984; Bothun, Schommer & Sullivan 1984; Gavazzi & Jaffe 1987; Gavazzi 1989; Sun & Vikhlinin 2005), it has been studied with MUSE by Consolandi et al. (2017) who found in the tail both diffuse emission and compact knots of low velocity dispersion with line ratios typical of H II regions, whose physical properties do not differ from normal H II regions in galactic discs.

(c) SOS 114372 (7×10^{10} $M_\odot$) in the Shapley Abell 3558 cluster was studied using Wifes IFU data by Merluzzi et al. (2013) who found Hα knots and filaments in the one-sided 13kpc ionized gas tail, detecting a contribution from shock excitation as well as star formation. We note that this galaxy is the GASP galaxy JO147 presented in this paper, that was independently identified as a gas stripping candidate by Poggianti et al. (2016).

In addition, detailed GASP studies of five individual galaxies showing star formation in the tails were published in Poggianti et al. (2017b); Bellhouse et al. (2017); Fritz et al. (2017); Gullieuszik et al. (2017); Moretti et al. (2018a), Bellhouse et al. in prep, see these papers for details.

In the absence of IFU or spectroscopic data, strong evidence for ongoing SF in the tails can come from Hα narrow-band observations in combination with UV data. The latter, if sufficiently deep, can reveal the stellar knots formed in the tails and therefore confirm that the Hα emission is due to ongoing SF, and viceversa Hα can confirm

that the UV knots belong to the galaxy and are not background sources. Well-studied individual cases are:

(d) NGC 4254 (2.4×10^{10} M$_\odot$), in the Virgo cluster, in which Boselli et al. (2018) has identified 60 GALEX candidate star forming regions up to 20 kpc outside of the disc, of which 30 have also Hα emission. The 250 kpc HI tail of this galaxy seems to be driven by a recent gravitational encounter with another Virgo member, and the knots in the tail are interpreted as coeval knots formed after a single SF burst.

(e) NGC4330 (6×10^9 M$_\odot$) in Virgo, in which extraplanar UV regions close to the disc were found by Abramson et al. (2011), who interpret them as extraplanar star formation in a galaxy undergoing initial stripping, that has yet to reach peak stripping. Star-forming extraplanar regions are also visible in Hα imaging (Abramson et al. 2011; Fossati et al. 2018).

Moreover, another Virgo dwarf galaxy, VCC1249 (1.2×10^9 M$_\odot$), interacting with a massive elliptical companion, shows that the combination of tidal interaction and ram pressure stripping led to the removal of HI gas from the disc and that extraplanar H II regions were formed in situ in the gas removed (Arrigoni et al. 2012).

To our knowledge, the only case for which it has been argued that no star formation occurs in a long tail with Hα emitting gas is NGC4569 (3×10^{10} M$_\odot$) in Virgo, which has an 80kpc long Hα tail and is affected both by ram pressure and a strong close interaction. Boselli et al. (2016) argue that no star forming region is observed in the tail and conclude that other mechanisms other than photoionization (such as shocks, heat conduction or magnetohydrodynamic waves) are responsible for the emission.

Two very well-studied cases of galaxies in a 'post-stripping' phase in which there is little star formation left but the stellar knots previously formed in the tails are still strikingly visible are:

(f) IC3418 (4×10^8 M$_\odot$), a post-starburst passive galaxy in Virgo, with a 17kpc tail of UV knots that were recognized as star-forming regions and characterized by Hester et al. (2010); Fumagalli et al. (2011); Kenney et al. (2014). IC3418 has little ionized gas left only in the outer tail. This galaxy also has a possible marginal detection of $\sim 10^6$ M$_\odot$ of molecular gas in the disc, and only CO upper limits in the tail (Jáchym et al. 2013).

(g) RB199 (8×10^8 M$_\odot$, Sun et al. 2010), another post-starburst disc but in the Coma cluster, very similar to IC3418 in many ways (Yoshida et al. 2008). This is a galaxy–galaxy merger remnant whose gas tail is ascribed to ram pressure and whose 80kpc tail shows UV and Hα bright knots forming stars.

Other strong evidence for star formation in stripped tails comes from the works of Smith et al. (2010) and Yagi et al. (2007); Yagi & Fukahata (2008); Yagi et al. (2010) in the Coma cluster. Smith et al. (2010) showed with GALEX data that 13 star-forming galaxies have tails with filaments and knots concluding that SF occurs within the stripped gas by interaction with the cluster environment, presenting also HST data for two of these that reveal compact blue knots coincident with UV and Hα emission. Yagi and collaborators mapped Coma with Hα imaging, and found Hα clouds associated with 14 Coma members (6 of which belong to the Smith et al. sample). Some of these clouds are connected with disc SF, some are clouds connected to a disc that is devoid of SF (e.g. like IC3418 and RB199) and some others are totally detached clouds. Extended ionized gas clouds, some of which are associated with galaxies, some not, have also been detected in Abell 1367 by Gavazzi et al. (2001) and Yagi et al. (2017).

Indirect support for the probable presence of SF in stripped tails comes from the detection of a large amount of molecular gas in the tail of D100 (2×10^9 M$_\odot$) in Coma (Jáchym et al. 2017) within the 60kpc long Hα + UV tail studied by Yagi et al. (2007, 2010), and Smith et al. (2010).

Molecular gas is also present along the tail of NGC4388 (Verdugo et al. 2015), a Virgo galaxy in which in situ star forming regions were found in the tail by Yagi et al. (2013) based on photometric data and slit spectroscopy. This galaxy is an interesting case for having both an HI tail and a faint X-ray tail (Oosterloo & van Gorkom 2005; Sun et al. 2010; Boissier et al. 2012). Some molecular gas was also detected close to the giant elliptical M86 in Virgo, but it was difficult to find a secure association with the neighboring galaxies (including NGC4388) (Dasyra et al. 2012).

Finally, Cortese et al. (2007) studied two dwarf galaxies in two clusters at z = 0.2 with HST finding tails with bright knots and stellar streams that the authors interpreted as star-forming knots consistent with the formation of ultracompact dwarf galaxies. At even higher redshifts, again HST revealed bright blue knots consistent with star formation in the debris tails of jellyfishes in clusters (Owen et al. 2006; Owers et al. 2012; Ebeling, Ma & Barrett 2014).

We note that at odds with several of the well studied cases in Virgo, galaxies clearly interacting with a nearby companion have been excluded from our sample. Concerning the SF in the tails, our GASP results are very much in line with previous findings, and extend them to a larger, homogeneously observed sample for which IFU spectroscopy allows to study the ionization mechanisms in the tails and the physical properties of the star forming clumps. They are formed in low velocity dispersion gas, as found by previous studies (e.g. Fumagalli et al. 2014; Fossati et al. 2016; Consolandi et al. 2017). The tail clumps in our sample extend to higher Hα luminosities and stellar masses than those identified by Boselli et al. (2018) in NGC 4254 ($L_{\rm H\alpha} = 10^{37} - 10^{38}$ erg s^{-1}, $M = 10^3 - 10^5$ M$_\odot$) and by Smith et al. (2010) in their two galaxies with HST data ($M = 10^4 - 10^5$ M$_\odot$), but similar Hα luminosities to the clumps in ESO137-001 (Sun et al. 2007) and similar stellar masses and SFRs to the clumps in RB199 in Coma ($M = 10^6 - 10^7$M$_\odot$ Yoshida et al. 2008). Generally, the clumps presented in this paper extend to higher masses than those in ram pressure stripped tails in Virgo (see Yagi et al. 2013, and references therein). The characteristics of the clumps formed in the tails are expected to depend on the ICM physical conditions. For example, the ICM in Virgo is 10 times less dense and hot than in Coma, and higher density and pressure can help the gas confinement and the SF in the tails. On the other hand, our results demonstrate that tail SF does not occur only in very massive clusters, but also in low mass clusters with $\sigma = 500 - 600$ km s^{-1} where some of our most spectacular cases are found (e.g. JO204, JO206, see Table 1). We also note that, with the exception of SOS114372/JO147, no jellyfish with a mass higher than $3 \times 10^{10} M_\odot$ was studied in detail before GASP. However, SF does not occur only in the tails of galaxies of a given mass range, as demonstrated by the fact that we detect it in galaxies with a wide range of stellar masses ($3 \times 10^9 - 3 \times 10^{11}$ M$_\odot$, Table 1), although the net amount of tail SF depends on galaxy mass, as we discuss in Gullieuszik et al. (in prep.).

8.2 Expectations from hydrodynamical simulations

A few simulations have examined star formation in ram pressure stripped tails. Most agree that star formation can take place throughout the tail as at any time stripped gas will have a range of densities and temperatures that will be accelerated at different rates and have

different collapse timescales (Kapferer et al. 2009; Tonnesen & Bryan 2012; Roediger et al. 2014; but Steinhauser, Schindler & Springel 2016 find no star formation in their tails).

Kapferer et al. (2009) ran 12 simulations varying the ram pressure wind velocity and density, and found that increasing the ram pressure increases the SFR in the tail. The SFR was more strongly affected by the wind density than the wind velocity. Tonnesen & Bryan (2012) also argued that the SFR in the tail increased with increasing surrounding ICM thermal pressure. In Jaffé et al. (2018), we found that the longest and most strongly star-forming tails tended to be moving quickly near the center of clusters. The simulations indicate that it is the surrounding dense ICM that is driving the high SFRs in these tails. The high velocities of the galaxies towards the centre of the cluster allow for gas to travel farther from the galaxy before it collapses and forms stars.

The average SFR over 500 Myr in the Kapferer tails ranged from 0.2–2 $M_\odot\,yr^{-1}$, depending on the ram pressure strength. The SFR was much lower in the Tonnesen & Bryan (2012) tail, peaking at about 0.06 $M_\odot\,yr^{-1}$. As discussed in Tonnesen & Bryan (2012), there are many differences in the codes and initial conditions used in the simulations that will affect the SFRs found in different works. The total SFR we measure in tails (column 3 of Table 3) ranges between ∼0.01 and $1M_\odot\,yr^{-1}$, with a median of 0.20 $M_\odot\,yr^{-1}$ (Q1 = 0.03, Q3 = 0.44), in agreement with the ranges spanned by the simulations.

Tonnesen & Bryan (2012) also considered the stellar clumps formed in tails. Using the Kennicutt's (1998a) relation to go from SFR to Hα luminosity, the authors found that the brightest clumps have an Hα surface brightness $< 3 \times 10^{38}$ erg s^{-1} kpc^{-2}, and only the few most massive stellar clumps have mass surface densities of 3×10^4 $M_\odot$ kpc^{-2}. A comparison with our observed values will need a careful assessment of spatial resolution effects both in observations and simulations. We will use simulations to examine how clump properties are related to the surrounding ICM in future work.

9 SUMMARY

In this paper, we have presented the analysis of the MUSE data of 16 cluster galaxies with clear tails of ram pressure stripped gas from the GASP survey. All galaxies present bright Hα clumps in their tails as well as interclump regions of more diffuse emission. We have found that:

(1) The ionization mechanism of the tails has been investigated using three different emission line ratio diagnostic diagrams. Such mechanism could be derived for all spaxels with sufficiently high *S/N* data, which on average account for about 60 per cent of the total Hα luminosity in the tails.

According to the N II and S II diagnostic diagrams, the fraction of Hα luminosity in the tails powered by SF ranges from galaxy to galaxy between ∼70 per cent and 100 per cent, with a median fraction of about 90 per cent. When using the OI DD, the SF-powered fraction ranges between 87 per cent and 12 per cent depending on the galaxy, with a median of 64 per cent. The [O I] diagram is the most sensitive one to a contribution from shocks, but in the stripped tails the extra [O I] emission might be due to thermal heating of the stripped gas by the hot ICM.

(2) Timescale arguments rule out the possibility that the photons ionizing the gas in the tails originate from massive stars in the discs of these galaxies. Based on this, as well as on our molecular gas detections in the tails (Moretti et al. 2018b) and our deep FUV and NUV imaging (George et al. 2018), we conclude that star formation occurs in situ in the tails, within the Hα clumps we identify.

(3) The DD analysis of the integrated spectra of Hα clumps finds that the vast majority of clumps in the tails are powered by SF, or SF + Composite emission, and have gaseous velocity dispersions $< 50\,km\,s^{-1}$. Clumps with high emission line ratios have instead $\sigma > 50$–$70\,km\,s^{-1}$, probably due to thermal conduction/turbulence effects and/or contamination by turbulent diffuse gas along the line of sight.

(4) The Hα star-forming clumps in the tails resemble giant and supergiant H II regions and complexes, with a median gas velocity dispersion of 27 km s^{-1} and Hα luminosities in the range 10^{38}–10^{39} erg s^{-1}.

(5) We measure moderate values of dust extinction in the clumps (median $A_V = 0.5$ mag), which are lower on average than those of clumps in the discs. The SFR of clumps in the tails is also lower on average than in the discs (0.003 $M_\odot\,yr^{-1}$ versus 0.008 $M_\odot\,yr^{-1}$), but the SFR estimates are subject to large uncertainties due to the unknown IMF and stochastic effects in the IMF sampling at these low SFR values.

(6) The density of the gas can be measured from the [S II] lines in the MUSE spectra for about half of the clumps. Measured values show a wide density distribution, between 20 cm^{-3} and well above 100 cm^{-3}, with a median of ∼50 cm^{-3}, indicating that dense gas clumps are present in the tails.

(7) The ionized gas mass of the clumps, whose median is $4 \times 10^4 M_\odot$, broadly correlates with the stellar mass of the clumps (median $3 \times 10^6 M_\odot$). On the basis of their stellar masses, we speculate that the clumps formed in the tails of stripped gas contribute to the large population of UCDs/GCs/dSphs observed in nearby clusters, or even to the UDG population depending on their subsequent dynamical evolution.

(8) The clump SFR correlates well with both the clump gas mass and stellar mass. Interestingly, the clumps in the tails follow the exact same correlation between SFR and gas mass of clumps in the discs.

The star-forming clumps both in the tails and the discs roughly follow also the relation between gas velocity dispersion and Hα luminosity of low redshift star-forming galaxies. Assuming they also share the Hα luminosity-size relation of clumps in the discs of low-z spirals from the literature, we infer they should have typical core radii between 100 and 400 per cent, with a median of 160 per cent in the tails. These sizes are below our spatial resolution limit and require higher resolution studies.

(9) On average 50 per cent of the Hα luminosity in the tails is in the form of diffuse emission. We find a strong anticorrelation between the fraction of Hα tail emission that is diffuse and the total SFR in the tail.

The diffuse tail emission originates both from ionizing photons due to SF and from other mechanisms producing Composite or LINER-like emission line ratios. The relative contribution of SF and non-SF processes varies significantly when considering the N II and the OI DD, and from one galaxy to another.

Under the hypothesis that the ionizing photons responsible for the SF component of the diffuse emission originate within the star-forming clumps, we estimate an average escape fraction from the clumps of 18 per cent, ranging between 6 and 46 per cent from galaxy to galaxy.

(10) In most galaxies, the SFR in the tails represents only a small fraction (a few per cent) of the total SFR of the system (tail + disc). In the 6 galaxies with the longest tails this fraction is much higher,

between 10 and 20 per cent. Most of the SF in the tails is concentrated in the clumps.

To summarize, we detect ongoing star formation in the tails of all galaxies in our sample, that cover two orders of magnitude in galaxy stellar masses (between a few times 10^9 to a few times 10^{11} $M_\odot$) and are members of galaxy clusters with velocity dispersions between ∼550 and over a 1000 km s^{-1}, from low mass to very massive clusters.

In this work, we have demonstrated that SF occurring in-situ in the tails is a common phenomenon and started to unveil the physical properties of the star forming clumps in the stripped tails of a statistically significant sample of jellyfish galaxies. These tails are unique laboratories to study the star formation process, in the absence of an underlying galaxy disc and in a fully gas-dominated regime. Future works using the GASP MUSE data and its multiwavelength ongoing follow-ups (APEX, ALMA, JVLA and UVIT@ASTROSAT) will address some of the several questions this work has opened.

ACKNOWLEDGEMENTS

We are grateful to the anonymous referee for her/his constructive and detailed comments. We would like to thank Emily Wisnioski for providing us the data from her paper. This work made use of the KUBEVIZ software which is publicly available at http://www.mpe.mpg.de/∼dwilman/kubeviz/. We warmly thank Matteo Fossati and Dave Wilman for their help with KUBEVIZ. We are grateful to Oleg Gnedin, Frank van den Bosch, Elke Roediger, Bruce Elmegreen, Miroslava Dessauges-Zavadsky, Sally Oey, Rob Kennicutt, Roberto and Elena Terlevich and all the organizers and participants of the Ringberg 2017 conference on 'Galaxy evolution in groups and clusters at low redshift: theory and observations' (https://ringberg2017.wixsite.com/ap-ringberg2017) and of the Cambridge meeting on 'The laws of star formation: from the cosmic dawn to the present universe' (https://www.ast.cam.ac.uk/meetings/2018/sf.law2018.cambridge) for useful discussions. We acknowledge financial support from PRIN-SKA 2017 (PI L. Hunt). Y. J. acknowledges support from CONICYT PAI (Concurso Nacional de Inserción en la Academia 2017) No. 79170132. Based on observations collected at the European Organisation for Astronomical Research in the Southern Hemisphere under ESO programme 196.B-0578. Based on observations taken with the AAOmega spectrograph on the AAT, and the OmegaCAM camera on the VLT.

REFERENCES

Abramson A., Kenney J. D. P., Crowl H. H., Chung A., van Gorkom J. H., Vollmer B., Schiminovich D., 2011, AJ, 141, 164
Arrigoni M., Trager S. C., Somerville R. S., Gibson B. K., 2012, MNRAS, 424, 800
Bacon R., et al., 2010, SPIE, 7735, 773508
Bellhouse C. et al., 2017, ApJ, 844, 49
Biviano A. et al., 2017, A&A, 607, A81
Boissier S. et al., 2012, A&A, 545, A142
Boquien M. et al., 2009, ApJ, 706, 553
Boselli A. et al., 2016, A&A, 587, A68
Boselli A. et al., 2018, A&A, 614, A56
Bothun G. D., Schommer R. A., Sullivan W. T., III, 1984, AJ, 89, 466
Bournaud F., Duc P.-A., Amram P., Combes F., Gach J.-L., 2004, A&A, 425, 813
Bressan A., Marigo P., Girardi L., Salasnich B., Dal Cero C., Rubele S., Nanni A., 2012, MNRAS, 427, 127
Cardelli J. A., Clayton G. C., Mathis J. S., 1989, ApJ, 345, 245
Cava A. et al., 2009, A&A, 495, 707
Cava A., Schaerer D., Richard J., Pérez-González P. G., Dessauges-Zavadsky M., Mayer L., Tamburello V., 2018, Nature Astron., 2, 76
Chabrier G., 2003, PASP, 115, 763
Chung A., van Gorkom J. H., Kenney J. D. P., Vollmer B., 2007, ApJ, 659, L115
Conselice C. J., 2018, Res. Notes Am. Astron. Soc., 2, 43
Consolandi G., Gavazzi G., Fossati M., Fumagalli M., Boselli A., Yagi M., Yoshida M., 2017, A&A, 606, A83
Cortese L. et al., 2007, MNRAS, 376, 157
Crowl H. H., Kenney J. D. P., van Gorkom J. H., Vollmer B., 2005, AJ, 130, 65
da Silva R. L., Fumagalli M., Krumholz M., 2012, ApJ, 745, 145
da Silva R. L., Fumagalli M., Krumholz M. R., 2014, MNRAS, 444, 3275
Dasyra K. M., Combes F., Salomé P., Braine J., 2012, A&A, 540, A112
Drinkwater M. J., Jones J. B., Gregg M. D., Phillipps S., 2000, PASA, 17, 227
Duc P.-A., 2012, Astrophys. Space Sci. Proc., 28, 305
Ebeling H., Ma C.-J., Barrett E., 2014, ApJS, 211, 21
Elmegreen B. G., 2017, ApJ, 836, 80
Elmegreen B. G., Kaufman M., Thomasson M., 1993, ApJ, 412, 90
Elmegreen B. G., Elmegreen D. M., Sánchez Almeida J., Muñoz-Tuñón C., Dewberry J., Putko J., Teich Y., Popinchalk M., 2013, ApJ, 774, 86
Elmegreen D. M., Elmegreen B. G., Ravindranath S., Coe D. A., 2007, ApJ, 658, 763
Elmegreen D. M. et al., 2014, ApJ, 787, L15
Evans N. J., II, 1999, ARA&A, 37, 311
Ferland G. J. et al., 2013, RMxAA, 49, 137
Fossati M., Fumagalli M., Boselli A., Gavazzi G., Sun M., Wilman D. J., 2016, MNRAS, 455, 2028
Fossati M. et al., 2018, A&A, 614, A57
Franco J., Kurtz S. E., García-Segura G., Hofner P., 2000, Ap&SS, 272, 169
Fritz J. et al., 2017, ApJ, 848, 132
Fumagalli M., Gavazzi G., Scaramella R., Franzetti P., 2011, A&A, 528, A46
Fumagalli M., Fossati M., Hau G. K. T., Gavazzi G., Bower R., Sun M., Boselli A., 2014, MNRAS, 445, 4335
Gallagher J. S., Hunter D. A., 1983, ApJ, 274, 141
Gavazzi G., 1989, ApJ, 346, 59
Gavazzi G., Jaffe W., 1987, A&A, 186, L1
Gavazzi G., Tarenghi M., Jaffe W., Butcher H., Boksenberg A., 1984, A&A, 137, 235
Gavazzi G., Boselli A., Mayer L., Iglesias-Paramo J., Vílchez J. M., Carrasco L., 2001, ApJ, 563, L23
George K. et al., 2018, MNRAS
Gouliermis D. A. et al., 2017, MNRAS, 468, 509
Gullieuszik M. et al., 2017, ApJ, 846, 27
Gunn J. E., Gott J. R., III, 1972, ApJ, 176, 1
Hernandez S., Leitherer C., Boquien M., Buat V., Burgarella D., Calzetti D., Noll S., 2018, MNRAS, 478, 1292
Hester J. A. et al., 2010, ApJ, 716, L14
Hilker M., Infante L., Richtler T., 1999, A&AS, 138, 55
Jáchym P., Kenney J. D. P., Ržuička A., Sun M., Combes F., Palouš J., 2013, A&A, 556, A99
Jáchym P., Combes F., Cortese L., Sun M., Kenney J. D. P., 2014, ApJ, 792, 11
Jáchym P. et al., 2017, ApJ, 839, 114
Jaffé Y. L. et al., 2018, MNRAS, 476, 4753
Kapferer W., Kronberger T., Ferrari C., Riser T., Schindler S., 2008, MNRAS, 389, 1405
Kapferer W., Sluka C., Schindler S., Ferrari C., Ziegler B., 2009, A&A, 499, 87
Kauffmann G. et al., 2003, MNRAS, 346, 1055
Kenney J. D. P., van Gorkom J. H., Vollmer B., 2004, AJ, 127, 3361
Kenney J. D. P., Geha M., Jáchym P., Crowl H. H., Dague W., Chung A., van Gorkom J., Vollmer B., 2014, ApJ, 780, 119
Kennicutt R. C., Jr., 1998a, ARA&A, 36, 189
Kennicutt R. C., Jr., 1998b, ApJ, 498, 541
Kennicutt R. C., Evans N. J., 2012, ARA&A, 50, 531

Kewley L. J., Heisler C. A., Dopita M. A., Lumsden S., 2001, ApJS, 132, 37
Kewley L. J., Groves B., Kauffmann G., Heckman T., 2006, MNRAS, 372, 961
Krumholz M. R., 2014, Phys. Rep., 539, 49
Larson R. B., 1981, MNRAS, 194, 809
Lee J. H., Hwang N., Lee M. G., 2011, ApJ, 735, 75
Markwardt C. B., 2009, in Bohlender D. A., Durand D., Dowler P., eds, Astronomical Society of the Pacific Conference Series Vol. 411, Astronomical Data Analysis Software and Systems XVIII. Astronomical Society of the Pacific, San Francisco, p. 251
Merluzzi P. et al., 2013, MNRAS, 429, 1747
Monreal-Ibero A., Colina L., Arribas S., García-Marín M., 2007, A&A, 472, 421
Moretti A. et al., 2017, A&A, 599, A81
Moretti A. et al., 2018a, MNRAS, 475, 4055
Moretti A. et al., 2018b, MNRAS, 480, 2508
Mulia A. J., Chandar R., Whitmore B. C., 2015, ApJ, 805, 99
Mullan B. et al., 2011, ApJ, 731, 93
Norris M. A. et al., 2014, MNRAS, 443, 1151
Oey M. S., Kennicutt R. C., Jr., 1997, MNRAS, 291, 827
Oey M. S., Kennicutt R. C., Jr., 1998, PASA, 15, 141
Oosterloo T., van Gorkom J., 2005, A&A, 437, L19
Osterbrock D. E., Ferland G. J., 2006, Mercury, 35, 40
Owen F. N., Keel W. C., Wang Q. D., Ledlow M. J., Morrison G. E., 2006, AJ, 131, 1974
Owers M. S., Couch W. J., Nulsen P. E. J., Randall S. W., 2012, ApJ, 750, L23
Poggianti B. M. et al., 2016, AJ, 151, 78
Poggianti B. M. et al., 2017a, Nature, 548, 304
Poggianti B. M. et al., 2017b, ApJ, 844, 48
Proxauf B., Öttl S., Kimeswenger S., 2014, A&A, 561, A10
Relaño M., Peimbert M., Beckman J., 2002, ApJ, 564, 704
Rich J. A., Kewley L. J., Dopita M. A., 2011, ApJ, 734, 87
Rich J. A., Kewley L. J., Dopita M. A., 2015, ApJS, 221, 28
Roediger E., Brüggen M., Owers M. S., Ebeling H., Sun M., 2014, MNRAS, 443, L114
Schmidt M., 1959, ApJ, 129, 243
Schweizer F., 2009, in Richtler T., Larsen S., eds, Globular clusters - Guides to galaxies, Springer, Berlin Heidelberg, p. 331
Sharp R. G., Bland-Hawthorn J., 2010, ApJ, 711, 818
Smith R. J. et al., 2010, MNRAS, 408, 1417
Steinhauser D., Schindler S., Springel V., 2016, A&A, 591, A51
Sun M., Vikhlinin A., 2005, ApJ, 621, 718
Sun M., Jones C., Forman W., Nulsen P. E. J., Donahue M., Voit G. M., 2006, ApJ, 637, L81
Sun M., Donahue M., Voit G. M., 2007, ApJ, 671, 190
Sun M., Donahue M., Roediger E., Nulsen P. E. J., Voit G. M., Sarazin C., Forman W., Jones C., 2010, ApJ, 708, 946
Terlevich R., Melnick J., 1981, MNRAS, 195, 839
Tonnesen S., Bryan G. L., 2012, MNRAS, 422, 1609
Verdugo C., Combes F., Dasyra K., Salomé P., Braine J., 2015, A&A, 582, A6
Vulcani B. et al., 2017, ApJ, 850, 163
Vulcani B. et al., 2018a, MNRAS, 480, 3152
Vulcani B. et al., 2018b, ApJ, 852, 94
Vulcani B. et al., 2018c, ApJ, 866, L25
Wisnioski E., Glazebrook K., Blake C., Poole G. B., Green A. W., Wyder T., Martin C., 2012, MNRAS, 422, 3339
Wittmann C., Lisker T., Pasquali A., Hilker M., Grebel E. K., 2016, MNRAS, 459, 4450
Wofford A., Leitherer C., Salzer J., 2013, ApJ, 765, 118
Yagi Y., Fukahata Y., 2008, Geophys. J. Int., 175, 215
Yagi M., Komiyama Y., Yoshida M., Furusawa H., Kashikawa N., Koyama Y., Okamura S., 2007, ApJ, 660, 1209
Yagi M. et al., 2010, AJ, 140, 1814
Yagi M., Gu L., Fujita Y., Nakazawa K., Akahori T., Hattori T., Yoshida M., Makishima K., 2013, ApJ, 778, 91
Yagi M., Yoshida M., Gavazzi G., Komiyama Y., Kashikawa N., Okamura S., 2017, ApJ, 839, 65
Yoshida M. et al., 2008, ApJ, 688, 918

This paper has been typeset from a TEX/LATEX file prepared by the author.